

The Polycluster Theory for the Structure of Glasses: Evidence from Low Temperature Physics

Giancarlo Jug[*]

Dipartimento di Scienza ed Alta Tecnologia and To.Sca.Lab
Università dell'Insubria, Via Valleggio 11, 22100 Como, Italy
and INFN – Sezione di Pavia, Italy

March 2, 2022

Abstract

The problems of the intermediate-range atomic structure of glasses and of the mechanism for the glass transition are approached from the low-temperature end in terms of a scenario for the atomic organization that justifies the use of an extended tunneling model. The latter is crucial for the explanation of the magnetic and compositional effects discovered in non-metallic glasses in the Kelvin and milli-Kelvin temperature range. The model relies on the existence of multi-welled local potentials for the effective tunneling particles that are a manifestation of a non-homogeneous atomic structure deriving from the established dynamical heterogeneities that characterize the supercooled liquid state. It is shown that the extended tunneling model can successfully explain a range of experiments at low temperatures, but the proposed non-homogeneous atomic structure scenario is then tested in the light of available high resolution electron microscopy imaging of the structure of some glasses and of the behaviour near the glass transition.

1 Introduction

The physics of glass-forming liquids, especially at higher temperature, continues to generate considerable research effort. These substances of extraordinary practical and technological importance still present considerable scientific challenges in the description of the glass-formation mechanism (nature of the glass transformation) and of the nature of the atomic structure at intermediate- and long-range length scales that characterize the solid. Standard X-ray and other scattering techniques fail in this respect to give a conclusive answer about the atomic structure of topologically disordered solids and the development of new investigation tools is desirable since there is no way to distinguish via scattering the structure of the liquid from that of the topologically disordered solid except through the vastly different relaxation time scales. Opinions as to why divergent time scales characterize the formation of the topologically disordered solid differ, however, and no agreement on a justification from structure for the mechanical properties below the glass transformation temperature T_g has to date been reached. Why should indeed a microscopically liquid-looking assembly of interacting particles behave (mechanically) like a crystalline solid remains to date a true mystery. Owing to such difficulties much theoretical and computational research on the description of the topologically disordered solid and its properties takes its moves from the study of the corresponding liquid for which much has been understood thanks to equilibrium statistical mechanics. Though understandable, this approach would correspond to be wanting to understand the physical properties of a crystalline solid from the study of its melt, which of course would present some formidable challenges given the ergodicity-breaking phenomenon that characterizes crystallization. In this essay it is proposed that the glass transition is of a purely kinetic nature and the use of equilibrium statistical mechanics is at its very limit of applicability since ergodicity also gets broken, though perhaps not so sharply and completely as for crystals, through the onset of the glassy state. The idea is then to try to learn something about the structure below T_g and the kinetic character of the glass transition starting from the phenomenology of the better understood supercooled liquid state (defined for temperatures T in the range $T_g \leq T \leq T_c$, with T_c the (equilibrium) crystallization temperature) and folding that knowledge in the study of the low-temperatures properties of laboratory amorphous solids. The return to low-temperatures is for glasses in a sense akin to starting to study the crystalline solid through X-ray and other (e.g. neutron-) scattering techniques at “zero” temperatures assuming the atoms in fixed positions. However since at those temperatures the glass would look like a liquid in a static scattering experiment, one has to exploit other specific degrees of freedom of the cold, topologically disordered solid that are not present for the perfectly ordered crystals. These are the so-called tunneling systems (TSs), local defects described in terms of new local degrees of freedom and that can be exploited – much as the atomic nuclei in NMR research – to probe the atomic structure and properties of the glassy state. The only difficulty is that these TS probes are not entirely localized, each comprising several atoms as a rule, and have not been fully understood to date. However, progress in their characterization and in the understanding of their microscopic nature is advancing also in view of some recent challenges posed by the discovery of puzzling magnetic effects in non-magnetic glasses that cannot be attributed (despite some interesting attempts) to trace paramagnetic impurities. Moreover, in the strategic research for reliable solid-state qubits to be deployed for the fabrication of working quantum computers (e.g. through use of Josephson-junction superconducting devices) the problems posed by the TSs (ubiquitous in the junctions) are paramount. These new challenges foster enhanced research efforts that have culminated in the development of an extended tunneling model [1] that relies on a new scenario for the intermediate-range atomic structure of glasses. The new model and structural scenario afford a reasonable - though not complete - explanation for the low- T anomalies in glasses and in turns the structural scenario can be evolved at higher temperatures to formulate a possible mechanism for the onset of the glass transition from the supercooled state. Preliminary aspects of the structure that is expected are tested in this essay and seem to corroborate some known facts about the glassy state. In this new framework of ideas, research in the previously-exotic low- T regime begins to give very useful hints about the onset of the glassy state from the supercooled liquid at much higher temperatures. The interplay of knowledge coming from the high- T supercooled liquid state and from the low- T cryogenic properties thus begins to provide a productive symbiosis for the understanding of this still mysterious, though ubiquitous, state of matter.

At low temperatures (cryogenic) glasses are believed to be characterized by special low-energy excitations (TSs) which are usually described through the use of double-welled potentials (DWPs) and of so-called two-level systems (2LSs) with energy asymmetry and tunneling barrier broadly distributed throughout the mass of the amorphous solid [2, 3]. While little is still known about the character (atomic, polyatomic or cluster-like) of the TSs, the general agreement is still that the intermediate-range atomic structure of glasses should be conveniently well described by Zachariasen’s 1932 continuous random network (CRN) model [4, 5] (thus

homogeneously disordered, just like for a liquid) and the 2LSs therefore result out of two slightly similar, probably localized atomic configurations. With this by now classic characterization, the 2LSs have been employed mainly in the 1970s and 80s to explain with some success the anomalies in the physical properties of glasses at low and ultra-low temperatures, a research field thus far completely detached from the quest for the nature of the glass transition.

Yet, systematic deviations from the behaviour predicted by the standard tunneling model (STM) occasionally challenge (or have challenged) the validity of the model in the case of multi-component glasses with tunable content of the good crystal-forming (GCF) component (e.g. $(\text{SiO}_2)_{1-x}(\text{K}_2\text{O})_{1-x}$ with changing x , the concentration of the alkali component, [6, 7]) and especially in glasses of the compositions type $\text{BaO-Al}_2\text{O}_3\text{-SiO}_2$ and then in the presence of a weak magnetic field [8]. In such glasses (unfortunately the mixed alkali-silicate glasses have not yet been investigated in a field, but the prediction is important magnetic effects there, and x -dependent also) a puzzling non-monotonous magnetic-field dependence in many properties has been unveiled in some physical properties [9, 10, 11]. The magnetic effect is typically (but not always) weak, but orders of magnitude larger than expected from basic thermodynamic-science considerations. The STM by itself is unable to account for the compositional and magnetic effects, therefore a suitable extension of the celebrated tunneling model for both situations has been proposed by the present Author [1]. This so-called extended tunneling model (ETM) rests upon the existence (particularly in the multi-component glasses) of small regions of enhanced regularity (RERs) in the intermediate-range atomic structure of the somewhat incompletely-frozen (in fact) amorphous solid. A complete mathematical description and intimate physical justification of the ETM thus requires at the very least a partial (or complete) demise of the Zachariasen-Warren's vision of the intermediate-scale structure of glasses and amorphous solids in general.

As it happens, an alternative to the homogeneously-disordered approach of Zachariasen-Warren has been proposed and developed in the former Soviet Union and in some places in the West. Well before Zachariasen-Warren, Lebedev [12] and his followers in Skt. Petersburg (but Randall in London, UK, too [13]) proposed that glasses should be made up of (initially, true) polycrystallites of sufficiently small size as to justify the X-ray peak rounding which was observed experimentally in diffractometers. Since the thermal and mechanical properties of glasses are reported not the same as those of polycrystalline solids, the concept of "crystallite" has evolved, meaning finally a failed micro-crystal of some sort. Also because finite clusters cannot be crystalline, strictly speaking. The evolution of the crystallite concept can be found in reviews by Porai-Koshits (see, e.g., [14]) and the latest views rely on concepts such as "cybotactic groupings", meaning atomic regions that can be rather extended and interpenetrating, but where the atomic ordering - though not complete due to finite size, thus highly defective - is better achieved than in the rest of the solid. A recent overview can be found in the works by Wright [15], and in the Russian literature recent ideas have been put forward also by Bakai [16, 17]. The latter Author envisages in fact better-ordered clusters being preferentially nucleated below T_c through some kinetic mechanisms that have the clusters survive and grow at the expense of true micro-crystalline nuclei that have no time to grow. At the glass transition these ill-formed, but better-ordered clusters merge together and get to form a polycluster that is the macroscopic skeleton of the solid glass. Evidently, looser material is also present in a patchwork atomic structure, characterized by spatial and (above T_g) temporal heterogeneities.

In this review we provide a scenario for the intermediate-range atomic structure of glasses, the cellular model, which is very much reminiscent of the polycluster theory of Bakai and a formulation within which the phenomenological assumptions for the ETM's mathematical framework (given in several papers by the present Author) become completely - or at least to a large extent - justified. The cellular or polycluster model provides for a definitely more realistic mathematical formulation of this framework in terms of a tetrahedral four-welled tunneling quasi-particle potential, as said, the simplified triangular three-welled version of which is nothing but a poor-man's, probably rather realistic, version affording a much speedier mathematical description. Within this cellular approach to the structure of glasses the most significant local tunneling potentials (probably in terms of number density) turn out to be the DWPs, this for a single (or very few) atomic particle(s), and the said tetrahedral four-welled potential (TFWP) for a correlated cluster of $N \gg 1$ charged real atomic particles. A reasonable and very useful simplification for the TFWP is thus the replacement of the N interacting and tunneling atomic particles with a single fictive quasi-particle subject to a triangular tunneling potential (TWP) and carrying renormalized parameters (charge, magnetic threaded area, energy asymmetry as well as tunneling probability), quantum-mechanically moving about one face of the full tetrahedral potential. The renormalization gets fully justified by the proximity of (on average) four similarly quasi-ordered, close-packed atomic cells (RERs or better-ordered regions) and the reasonable assumption that most of the charged particles will avoid the interstice's tetrahedral potential's centre. We

present again, therefore, a brief mathematical description of the TWP and its quantum mechanics in those limits appropriate for practical applications. We then show the main results obtained for the description of the density of states (DOS) and the temperature and magnetic-field dependence for the specific heat of some specific glasses, then for the dielectric constant (real and imaginary parts) in the linear-response regime, and for the polarization echo - always in the presence of a magnetic field (limiting to results obtained for the multi-silicates).

With this scenario of the cellular, or polycluster structure of real glasses assimilated, the question of the description of the glass transition is one of the next challenges. Having nucleation theory, and for better-ordered or Bakai clusters in mind the growth of such clusters with a cooling rate κ can be considered and the temperature at which the polycluster appears is taken to be T_g . With some phenomenological assumptions in the light of standard Adam-Gibbs theory (where the RERs, or Wright's better-ordered clusters, appear as CRCs or coherently-rearranging clusters) [18], the dependence of T_g from κ is worked out and the known logarithmic dependence can be recovered.

The paper is organized as follows. In Section 2 we introduce the cellular model for the structure of glasses, now a complete departure from Zachariasen's continuous random-network model, and then examine the likely tunneling states that would emerge from such cellular picture, to conclude that only DWPs and TFWPs should be relevant for the physics of glasses below the glass transition temperature T_g . In Section 2 we also review the basic relevant quantum mechanics of the three-welled, poor man's version of the TFWP, a version that has been used to date to obtain a reasonable single explanation for all of the anomalies (and deviations from the STM predictions) due to composition changes and to the presence of a magnetic field. We also show how to evaluate the magnetic density of states (DOS) $g(E, B)$ and, in Section 3, we briefly review some of the magnetic-field dependent low-temperature physical properties that have been studied to date, such as the heat capacity $C_p(T, B)$ comparing with some of the published data for the multi-silicate glasses. We then do the same for the dielectric constant, real part ϵ' and (just comment on the) imaginary part ϵ'' as well, also showing some comparison with available data at low (kHz) frequency, and then we examine the application of the ETM to the explanation of some of the data for the polarization (or, electric) echoes in the silicates (only commenting about glycerol, for which case the ETM has been able to explain the so-called isotope effect, which is in fact a mere mass substitution effect). Section 4 contains a discussion on how the cellular model can be implemented to gain information on the size of the better-ordered cells making up the polycluster structure of amorphous solids. The typical values for the cell size extracted from low-temperature experiment parameters are then compared with available high resolution electron microscopy (HREM) imaging of insulating glasses that show such structure. It is shown that estimates from low temperatures and from HREM imaging compare reasonably well. A brief derivation of the model's prediction for the cooling rate dependence of T_g is also provided and this Section 4 contains also our Conclusions.

2 The Cellular Model for the Atomic Structure of Glasses and the Three-Welled Tunneling Potential

Glass-forming liquids are an important class of materials for technology and ubiquitous applications, nevertheless the atomistic structure of glass in relation to its physical properties remains a mystery. As stated in the Introduction, the widespread conception is that the atomic arrangement of a glass should be the same as that for a liquid, as is indeed implicit in Zachariasen's 1932 proposed continuous network picture [4, 5], which has been widely adopted by scholars (at least in the West, see below). This picture differs from that of a liquid only in that a dynamical arrest has occurred, without specifying its ultimate origin. Relaxation times diverge "near" T_g , but why? In a spin-glass the ultimate origin of dynamical arrest is magnetic frustration (with or without disorder), but for ordinary structural glasses it remains mysterious and an important open issue [19, 20, 21, 22]. In the opinion of the present Author, lack of justification for this arrest is the primary roadblock for the achievement of a theory of the glassy state encompassing all aspects of glass physics in every possible temperature range. As mentioned in the Introduction, prior to Zachariasen's scheme, however, the Soviet scientist A.A. Lebedev had proposed, in 1921, the concept of "crystallites" [12], small crystal-like (yet not truly ordered) regions jammed against each other in random orientation to contain altogether all (actually, almost all) atoms in the glassy substance. Later, Randall proposed that these be real micro-crystals and explained the rounded-up X-ray spectra from glasses in this manner [13]. However, the density of glasses is typically some 10% less than that of poly-crystalline aggregates and the thermal properties of glasses too cannot be explained by means of the Lebedev-Randall picture. Despite these observations, the East-West

dichotomy continued to these days. The Zachariasen-Warren model of glass structure was for instance criticized by Hägg [23] in the West right in the early days of X-ray crystallography and a good review of the status quo of this controversy has been recently provided by Wright [15] who concludes, from a re-analysis of X-ray and neutron-scattering data from many different covalent-bonded and network glasses that indeed so-called *cybotactic groupings* (better-ordered regions) may well be present and frozen-in in most glasses, particularly if multi-component (or - one could add - polymeric [24]). The formation of *polyclusters*, instead of jammed crystallites, in most glasses is the latest scenario by the Eastern school [16, 17], which is based on observations and kinetic reasoning. As nicely set out by Bakai [16], the incipient crystals forming at and below T_c (melting point) are in constant competition with kinetically swifter (for glass-forming liquids) embryo clusters (or crystallites) that can win thermodynamically and kinetically over crystals during a rapid enough quench forming a polycluster spanning the whole of the sample.

On the experimental side, the concept of de-vitrification has been gradually taking sway with reports of metallic glasses [25] and also of monocomponent high-coordination covalent solids, like amorphous Si, forming *paracrystals* in their amorphous solids [26]. Therefore, the stance will be taken in this new review that only the purest mono-component glasses may (perhaps) abide to the Zachariasen-Warren dogma of the continuous random-network model for a glass, whilst the vast majority of real glasses [27] will be organized differently at the intermediate-range atomic structure level. Solid-like fluctuations of finite size are, in fact, likely to form already around and below the crystallization temperature T_c , the formed solid-like clusters continuously breaking up and reforming in the supercooled state between T_c and T_g , which is indeed widely known to be characterised by the so-called dynamical heterogeneities (DH). The slower-particle regions of the DH are, in the present Author's view, to be identified with the solid-like (better-ordered) clusters and the faster-particle DH regions with the liquid-like (completely disordered) clusters that become thinner and thinner as T_g is approached. In this vision, the lower temperature glassy structure (now entirely solid-like) inherits the inhomogeneous DH structure of the supercooled state, the slower, solid-like better-ordered regions having grown to a limit size (e.g. a maximum average radius ξ_0) that is determined by the onset of the polycluster. The structure now proposed is a cellular-type arrangement of better-ordered atomic regions (regions of enhanced ordering, RERs) that can have complicated, maybe fractal, but definitely compact shapes with a narrow size distribution and the intervening regions (let's call them interstitials) between them populated by still fast-moving particles (normally charged and possibly dangling-bonded ions). The interstitial regions between the RERs are here the equivalent of the concept of *cages*, that is often discussed in the glass structure's literature (see e.g. [19]). We remark that a cellular-type structure was already embodied within the "crystallite" idea of Lebedev, but now no micro-crystals are claimed here to exist (except definitely in the ceramic-glasses case, to a good extent). The RERs are more like Wright's "cybotactic regions" [15] or Treacy's "paracrystals" [26] (there for a-Si, not a quenched-melt solid) and issue from the DH picture for the glass-forming supercooled liquid state above T_g (see e.g. Fig. 1) [19, 28, 29, 30]. The DH picture does indeed recognise the presence of regions of "slower" and "faster" particles, and an inspection of the slower-particle regions of the supercooled liquid reveals that these are also better ordered (solid-like) whilst the faster-particle regions are rather much more liquid-like. DH are ubiquitous in perhaps all supercooled liquids [30] and the claim (though still somewhat speculative) here is that the slower-particle regions will grow on approaching T_g , albeit only up to a finite size and will now be giving rise to the RERs in the frozen, glassy state below T_g . In fact, simulations in the frozen glassy state of the slower- and faster-particle regions do confirm that a DH-like picture applies also below T_g [31] and with the slower-regions's size ξ increasing as $T \rightarrow 0$. Earlier simulations (always for model systems) [32] did point out the difficulty of simulating the DH picture below T_g and came up with a picture of these slower-regions growing, and possibly diverging in size, on approaching T_g . In the present review, however, the stance will be taken that the slower-regions' average (even maximum) size grows in real systems, but does not diverge at T_g or at any other characteristic temperature. Full experimental or numerical proofs of this fact are, unfortunately, still lacking and should be considered as a reasonable working hypothesis in this paper. Indeed, the absence of a diverging characteristic length is, in a nutshell, the central enigma of the problem of the glass transition. We remark in passing that a cellular structure (mosaic-like) for the glasses had been proposed by de Gennes [33] in the past and, in the context of the low-temperature anomalies, by Baltes [34] who was able to explain the linear in T anomaly in the heat capacity C_p (but not those in the acoustic properties, though, which require the introduction of tunneling). A very similar picture is that of the polyclusters of Bakai [16], as was already mentioned, but in the present approach the thermal genesis of the cells, or RERs, is ascribed directly to the DH scenario already present above T_g . In this approach the RERs, like grains or domains in the frozen structure below T_g , are the thermal-history continuation of the slower-particle regions of the DH above T_g . In Fig. 2 we show how

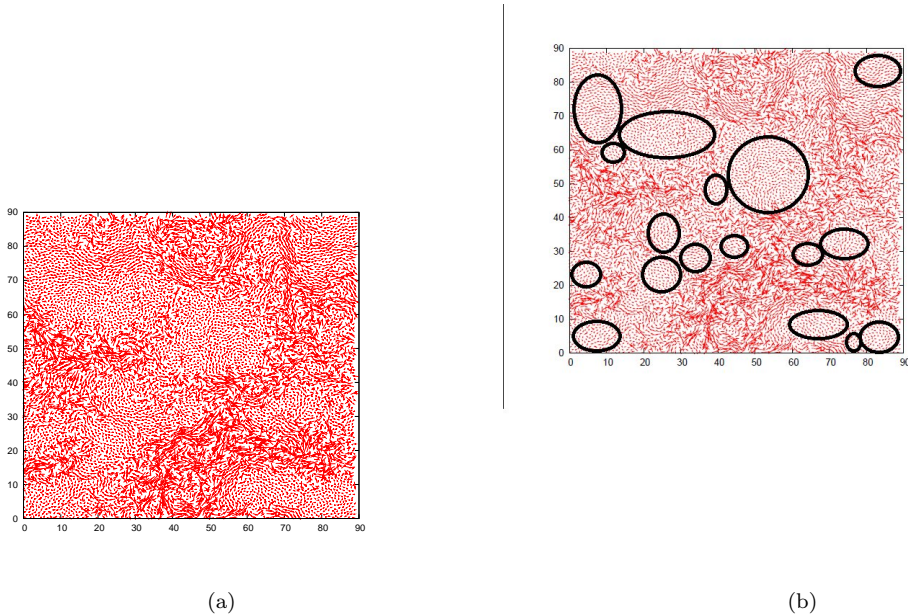


Figure 1: (a) Spatial map of a single-particle displacements in the simulation of a binary Lennard-Jones mixture in two dimensions. Arrows show the displacement of each particle in a trajectory of length comparable to the structural relaxation time. The map (courtesy of G. Biroli, from [19]) reveals the existence of particles with different mobilities during relaxation, also the existence of spatial correlations between these dynamical fluctuations. Faster and slower particle regions are clearly visible and a closer inspection reveals that the slower particles form better-ordered regions, while the faster particles form liquid-like regions. Note the distinct clustering of slow particles (dynamical heterogeneities, DH). (b) The slower regions have been schematically highlighted to show their incipient cellular structure. At the temperature of the simulation ($T > T_g$) the slower regions are continuously breaking up and reforming, the idea is that as T_g is approached their size grows to a finite limit value and their mutual hindering significantly slows down their dynamics. The ringed regions of slower moving particles become, below T_g , the RERs or cells characterizing glassy intermediate-range atomic structure.

the RERs themselves (and not the single particles) can get to grow to a limit intermediate-maximum size ξ_0 and randomly close-pack together in the proximity of the glass transition temperature T_g , thus forming a highly correlated polycluster. The random close-packing process gets to be completed at a lower temperature $T_K < T_g$ (T_K possibly to be identified with the Kauzmann temperature) thus giving the glass transition more the character of a crossover. As temperature drops further below T_K , the cells or RERs can slightly increase in size, consolidating their growth at the expense of the species present in the interstitials between the RERs. This idea of consolidation at lower temperatures is shown pictorially in Fig. 3. The cells and interfaces between the cells will contain the bulk of the tunneling systems. These 2LSs are atomic tunneling states arising from the cells' own disorder, but most of the 2LSs should be located at the meeting point between two cells (two RERs). In the interstitial spaces between cells the remnant faster particles of the DH at $T > T_g$ give rise for $T < T_g$ to regions where a large number N (on average, per interstitial) of charged atomistic tunneling particles are constrained to move in a coherent fashion due to the high Coulomb repulsion forces between them. Fig. 4 shows in a schematic way how the atomic/ionic matter can get organised below T_g in a real glass. Since the charged ions (dangling bonds, most likely) should act as a coherently tunneling ensemble, it seems natural to simplify the description of the physics at the lower temperatures using only phonons, propagating in the collection of cells now jammed against each other, and remnant ergodic localized degrees of freedom acting as TSs. These TSs will be of two types: the 2LSs within the cells and at their points of contact (owing to inherent disorder in the cells' atomic arrangement) and effective quasi-particles sitting in the close-packed cells' interstices and now representing the collective motion of the coherently-tunneling ions which are trapped in each interstice (Fig. 4). The quasi-particle will be subjected to an effective potential of distorted tetrahedral topology characterized by four wells for each RER interstice, with minima inside each RER or - depending on the material - at the RER meeting points and a high barrier in the interstice's

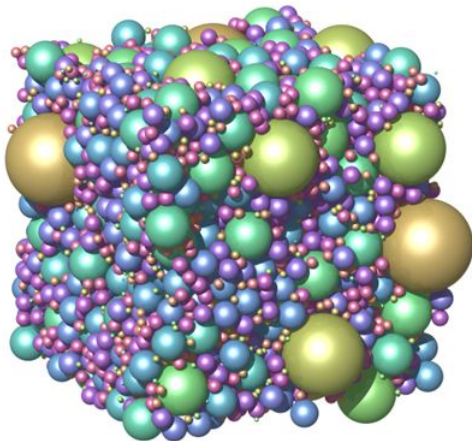


Figure 2: Random close packing of compact RERs in the proximity of the glass transition temperature T_g . The spheres represent regions of better-ordered atomic particles that have grown to a limit maximum size and hinder each other's further growth. In the interstitial regions (voids between the spheres), not shown, are the remainder of the incipient glass particles: these are more liquid-like and mobile, while the RERs that are shown need not be spherical nor completely mutually exclusive, partial coalescence being allowed.

centre. *De facto* this 3D interstitial TFWP potential can be replaced by four local 2D potentials for the four quasi-particles describing the coherent tunneling of the faster-moving particles sitting near each face of the distorted tetrahedron, close to a group of three (on average) quasi-ordered cells (Fig. 5). Because of the better-ordering implicit in this model of the glassy intermediate-range atomic structure, and in each cell, the three wells of each effective local 2D potential for the tunneling quasi-particles (four per interstice, on average) should be near-degenerate in terms of their ground-state energy asymmetries: $E_1 \simeq E_2 \simeq E_3 \simeq 0$. With this, still qualitative, picture in mind we now turn to the mathematical description of the physics of the remnant and still ergodic degrees of freedom (phonons in the cells' network - likely the origin of the Boson peak - 2LSs and ATs (anomalous tunneling systems, four in each interstice)). For our model of a real glass, by construction the 2LSs will be much more numerous than the ATs.

In this approach [1] the relevant degrees of freedom, beside the phonons, are generalised dilute gases of independent 2LSs described by the STM and of fictitious quasi-particles tunneling in TWP. The formulation of the STM (the 2LS model) for the low temperature properties of glasses is very well known [2, 3]. One assumes a collection of DWPs distributed in the substance and represented each by a 2×2 effective Hamiltonian of the form, in the potential-well (or real-space) representation:

$$\mathcal{H}_{2LS} = -\frac{1}{2} \begin{pmatrix} \Delta & \Delta_0 \\ \Delta_0 & -\Delta \end{pmatrix}. \quad (1)$$

Here the two parameters Δ (the energy asymmetry) and Δ_0 (twice the tunneling parameter) are typically characterized by a probability distribution that views Δ and $\ln(\Delta_0)$ (the latter linked to the particular DWP energy barrier) broadly (in fact, uniformly) distributed throughout the topologically disordered solid [35]:

$$\mathcal{P}_{2LS}(\Delta, \Delta_0) = \frac{\bar{P}}{\Delta_0} \quad (2)$$

where some cutoffs must be introduced when needed and where \bar{P} is an elusive material-dependent parameter, like the cutoffs. In fact, Eq. (2) embodies entirely the Zachariasen-Warren hypothesis for the intermediate atomic structure of a glass, assuming broadly-distributed the energy asymmetry $\Delta = E_2 - E_1$, hence the single-well ground state energies E_1 and E_2 themselves, as well as the potential barrier height V_0 appearing typically in relations such as:

$$\Delta_0 \simeq \hbar\Omega e^{-\frac{d}{\hbar}\sqrt{2mV_0}} \quad (3)$$

$$\Delta_0 = \frac{\hbar\Omega}{2} \left[3 - \sqrt{\frac{8V_0}{\pi\hbar\Omega}} \right] e^{-2\frac{V_0}{\hbar\Omega}} \quad (4)$$

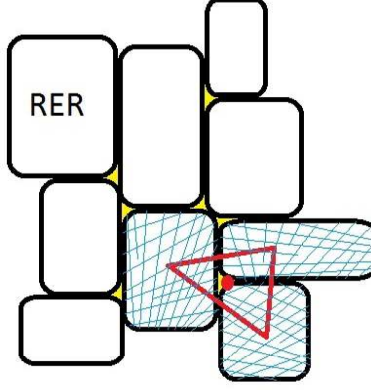


Figure 3: 2D cartoon of the consolidation of the RERs at the lower temperatures, where the better-ordered regions have grown at the expense of the particles in the interstitials. Ultimately this leads to a temperature-dependent number of liquid-like tunneling particles in each interstitial.

Here, the first relation is the generic WKB result for an arbitrarily shaped DWP (where m is the particle's mass, Ω its single-well harmonic frequency (or tunneling attempt frequency) and d the tunneling distance) and the second formula refers instead to a symmetric ($\Delta = 0$) DWP made up by two superimposed parabolic wells. In fact, in the end the distribution (2) refers to the combination of parameters $\Delta_0/\hbar\Omega$. The energies of the two levels $|0\rangle$ and $|1\rangle$ are then given by $\mathcal{E}_{0,1} = \pm \frac{1}{2}\sqrt{\Delta^2 + \Delta_0^2}$, and so on [2, 35].

The tunneling Hamiltonian of a particle in a TWP is also easily written down, in the same low- T spirit as for a 2LS, as a generalization of the above matrix formulation to the case of three wells [1]:

$$\mathcal{H}_{3LS} = \begin{pmatrix} E_1 & D_0 & D_0 \\ D_0 & E_2 & D_0 \\ D_0 & D_0 & E_3 \end{pmatrix} \quad (5)$$

where E_1, E_2, E_3 are now the energy asymmetries between the wells and where D_0 is the most relevant tunneling amplitude (through saddles of the glassy potential energy landscape, or PEL, in fact). No disorder in D_0 is considered, for simplicity, within each single DWP. This 3LS Hamiltonian has the important advantage of readily allowing for the inclusion of a magnetic field $B > 0$, when this is coupling orbitally with a tunneling “particle” (in fact, a quasi-particle) having charge q (q being some multiple of the electron's charge e) [1]:

$$\mathcal{H}_{3LS}(B) = \begin{pmatrix} E_1 & D_0 e^{i\varphi/3} & D_0 e^{-i\varphi/3} \\ D_0 e^{-i\varphi/3} & E_2 & D_0 e^{i\varphi/3} \\ D_0 e^{i\varphi/3} & D_0 e^{-i\varphi/3} & E_3 \end{pmatrix} \quad (6)$$

where $\varphi/3$ is the so-called Peierls phase for the tunneling particle through a saddle and in the field, and φ is the Aharonov-Bohm (A-B) phase for a tunneling loop (triangular shaped) and is given by the usual formula:

$$\varphi = 2\pi \frac{\Phi}{\Phi_0}, \quad \Phi_0 = \frac{h}{|q|} \quad (7)$$

Φ_0 being the appropriate magnetic flux quantum (h is Planck's constant) and $\Phi = \mathbf{B} \cdot \mathbf{S}_\Delta$ the magnetic flux threading the area S_Δ and formed by the tunneling paths of the particle in this now simplified (poor man's, yet as we have seen realistic) model. The three energy asymmetries E_1, E_2, E_3 typically enter through their natural combination $D \equiv \sqrt{E_1^2 + E_2^2 + E_3^2}$.

For $n_w=3$ wells an exact solution for the $k=0, 1, 2$ eigenvalues of the multi-welled tunneling Hamiltonian Eq. (6) is still possible (but not in the $n_w=4$ TFPW case):

$$\begin{aligned} \mathcal{E}_k &= 2D_0 \sqrt{1 - \frac{\sum_{i \neq j} E_i E_j}{6D_0^2}} \cos\left(\frac{1}{3}\theta + \theta_k\right) \\ \cos \theta &= \left(\cos \varphi + \frac{E_1 E_2 E_3}{2D_0^3}\right) \left(1 - \frac{\sum_{i \neq j} E_i E_j}{6D_0^2}\right)^{-3/2} \end{aligned} \quad (8)$$

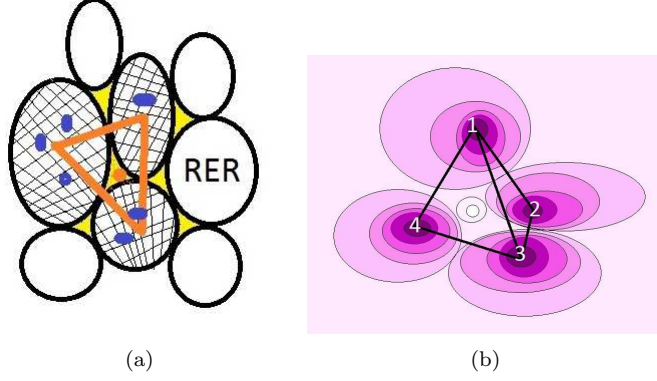


Figure 4: (a) A 2D cartoon of the cellular structure of an amorphous (melt-quenched) solid just below T_g . The RERs (black-circled blobs, an oversimplified schematics for fractal-like, but compact objects) have grown to completely fill the space and enclose atomistic tunneling states of the 2LS type (blue blobs). At the same time, in the RER interstitials (yellow regions, connecting to each other) the trapped, charged and faster particles of the DH existing above T_g (now probably charged dangling bonds), give rise to coherently-tunneling large groups of ions here represented by a single, fictitious, quasi-particle (orange dot) subjected to an effective tunneling potential having typically four natural wells in distorted-tetrahedral configuration (b) for close-packed RERs. (b) The tetrahedral four-welled potential (TFWP) in a 3D representation with a colour-coded potential intensity (dark=deepest, light=highest).

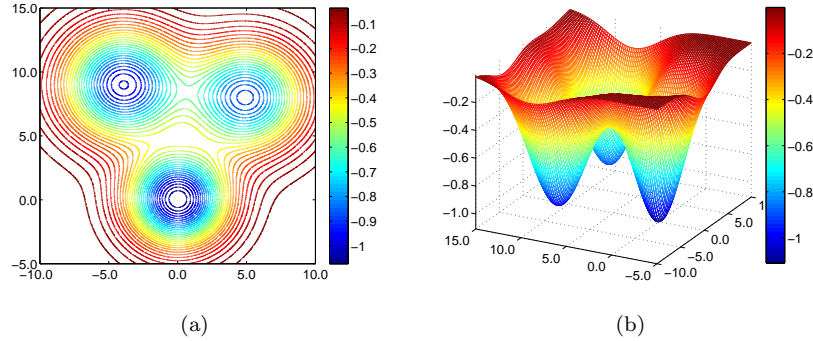


Figure 5: (a) Contour-plot of a possible realization of the 2D effective three-welled potential (TWP) very likely felt by the quasi-particle of those charged real particles dangling from, or being trapped by, a group of three RERs on each one face of the tetrahedral configuration for an interstice formed by close-packed RERs well below T_g (and T_K). (b) 3D attempted visualization of the same example of a TWP potential.

$\theta_k = 0, +\frac{2}{3}\pi, -\frac{2}{3}\pi$ an index distinguishing the three eigenstates. In the physically relevant limit, which we now consider, and in which $\varphi \rightarrow 0$ (weak fields) and $D = \sqrt{E_1^2 + E_2^2 + E_3^2} \rightarrow 0$ (near-degenerate distribution), and always at low temperatures, we can approximate (in a now simplified calculation) the $n_w = 3$ - eigenstate system with an *effective 2LS* having its energy gap $\Delta\mathcal{E} = \mathcal{E}_1 - \mathcal{E}_0$ widening with increasing φ provided $D_0 > 0$ (see below):

$$\lim \Delta\mathcal{E} \simeq \frac{2}{\sqrt{3}} \sqrt{D_0^2 \varphi^2 + \frac{1}{2}(E_1^2 + E_2^2 + E_3^2)} \rightarrow \sqrt{D_0^2 \varphi^2 + D^2} \quad (9)$$

(a trivial rescaling of D_0 and of the E_i has been applied). One can easily convince oneself that if such TWP is used and with the standard parameter distribution, Eq. (2) (with D, D_0 replacing Δ, Δ_0) for the description of the TS, one would then obtain essentially the very same physics as for the STM's 2LS-description. In other words, there would be no need to complicate the popular, minimal 2LS-description in order to study glasses at low temperatures, unless structural inhomogeneities of the RER-type and a magnetic field are present. Without the RERs, hence no distribution of the type (10) below, the phase interference from separate tunneling paths is only likely to give rise to an exceedingly weak quantum effect. Hence, it will be those TSs nesting between the RERs that will give rise to an enhanced quantum phase interference and these

TSSs can be minimally described – most appropriately and conveniently – through Hamiltonian (6) and with a distribution of asymmetries thus modified in order to favour near-degeneracy [1]:

$$\mathcal{P}_{3LS}^*(E_1, E_2, E_3; D_0) = \frac{P^*}{D_0(E_1^2 + E_2^2 + E_3^2)} \quad (10)$$

P^* being a dimensionless (which is pleasing) material parameter. We remark that the incipient “crystallinity” (better-ordering, in fact) of the RERs calls for near-degeneracy in E_1, E_2, E_3 simultaneously and not in a single one of them, whence the correlated form of (10). We now have basically three-level systems (3LSs) with energy levels $\mathcal{E}_0 < \mathcal{E}_1 \ll \mathcal{E}_2$, periodic in φ . The typical ATS spectrum, with $D_0 > 0$ (see below), is shown in Fig. 6 as a function of φ and one can now see that the third and highest level \mathcal{E}_2 can be safely neglected for most low-field applications. Other descriptions, with TFWPs or modified three-dimensional DWPs are possible for the TSSs nested in the RERs and yet they lead to the same physics as that from Eqs. (6) and (10) above (which describe what we like to call the anomalous tunneling systems, or ATSS, nesting in the interstitials between the RERs). The final and a most important consideration for the construction of a

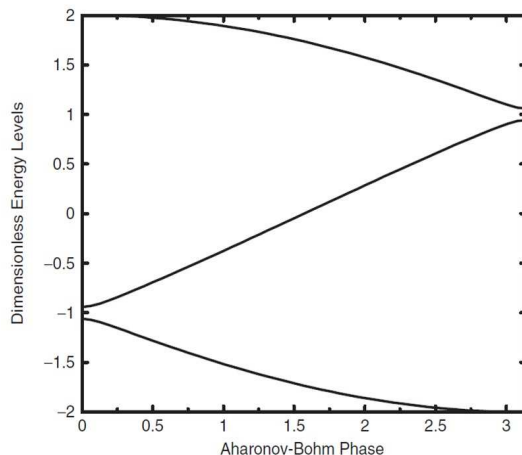


Figure 6: The energy spectrum (for $D_0 = 1$ units) of the ATS (3LS, TWP) model, in the physically appropriate limits of a weak magnetic field and near-degeneracy due to the embedding within RER’s interstitials. On the horizontal axis is the A-B phase $\varphi \propto B$.

suitable mathematical model of such complex systems is that the TSSs appear to be rather diluted defects in the glass (indeed their concentration is of the order of magnitude of that for trace, paramagnetic (e.g. Fe), impurities, as we shall see). Hence the tunneling “particles” are, de facto, embedded in a medium otherwise characterized only by fairly simple acoustic-phonon degrees of freedom. This embedding, however, does mean that the rest of the material takes its part in the making of the tunneling potential for the TSS’s “particle”, which itself is not moving quantum-mechanically in a true vacuum. Sussmann [36] has shown that this should lead to local trapping potentials that (for the case of triangular and tetrahedral perfect symmetry, like in our limit no-disorder case) must be characterized by a degenerate ground state. This should mean that, as a consequence of the TSS embedding, our poor man’s model, Eq. (6), for the ATSS should be chosen with a strictly positive tunneling parameter [1]:

$$D_0 > 0 \quad (11)$$

where of course perfect degeneracy gets always removed through weak disorder in the asymmetries. Intrinsic near-degeneracy of (10) of course implies that the model should be used in its $D/D_0 \ll 1$ limit, and that in turn reduces the ATSSs to effective magnetic-field dependent 2LSs, greatly simplifying the mathematical analysis when the limit $\varphi \rightarrow 0$, which we always take for relatively weak magnetic fields, is used. The ETM was first proposed in [1], and consists basically in a collection of independent, non-interacting 2LSs which are described by the STM and also 3LS-TWPs, which are described by Eqs. (6) and (10) above, in the mentioned $D/D_0 \ll 1$ and $\varphi \rightarrow 0$ limits. The 3LSs are meant to be nested in the interstitials between the close-packed RERs while the magnetic-field insensitive 2LSs are distributed in the remaining homogeneously-disordered granular matrix of RERs and at their touch points or interfaces [37]. In Fig. 7 we illustrate the behaviour of the magnetic part of the density of states (DOS) for this model as a function of the ATS gap energy, E , for different values of the A-B phase φ . This figure demonstrates the physical origin of the magnetic effects:

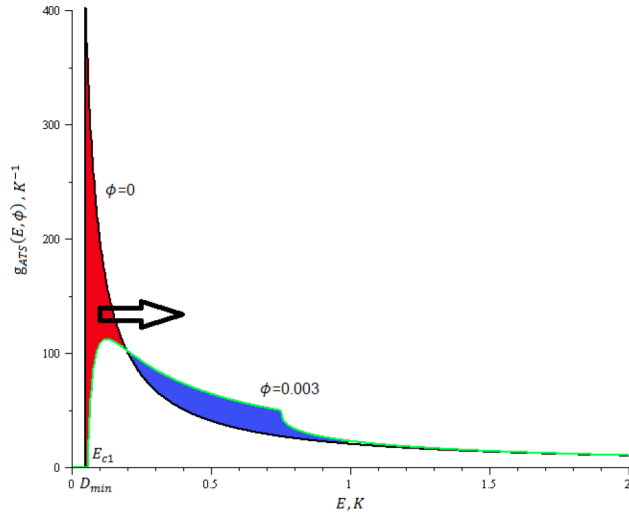


Figure 7: The magnetic-sensitive contribution of the density of states (DOS) as the function of the energy gap E and selected Aharon-Bohm (A-B) phases φ (proportional to the magnetic field B) (here $n_{ATS}P^*$ has been set to 1). The rapid transfer of quantum states to higher energy when a very weak magnetic field B is switched on is the basic explanation for the origin of the magnetic effects.

the number of quantum states being conserved, they get to be very rapidly shifted towards high values of the energy when a magnetic field, even very weak, is turned on. The ETM, proposed in this form by the

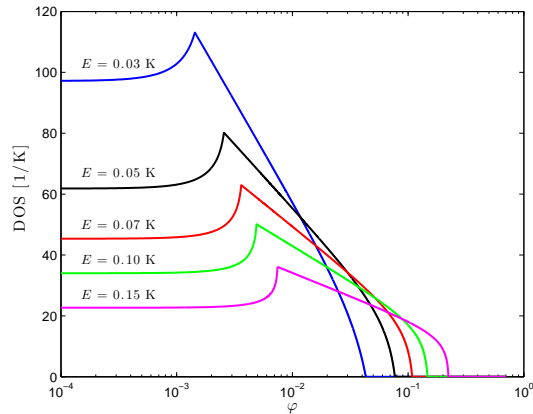


Figure 8: The magnetic-sensitive part of the density of states (DOS) as a function of the A-B phase φ (proportional to the magnetic field B , upon averaging) and different energies (again $n_{ATS}P^*$ has been set equal to 1). The shape of this DOS contribution (coming from the TWPs with a parameter distribution (10) which is favouring near-degeneracy) is the ultimate source of all the magnetic effects (see also Fig. 17). The cusp is an artifact of the effective 2LS approximation [1], albeit also of the existence of upper and lower bounds for D_0 due to the disordered nature of the RER glassy atomic structure.

present Author in 2004, has been able to explain so far the magnetic effects in the heat capacity [1], in the real [38] and imaginary [39] parts of the dielectric constant and in the polarization echo amplitude [39] data reported to date for a variety of glasses at low temperatures. The ETM has also shed much new light into the composition-dependent anomalies [7, 37]. The new physics provided by the magnetic-field dependent TS DOS, as mentioned, comes from a term due to the near-degenerate TWPs [1] and that gets to be added up

to the constant DOS from the STM 2LSs (having constant density n_{2LS}):

$$\begin{aligned} g_{tot}(E, B) &= n_{2LS}\bar{P} + n_{ATS}\frac{P^*}{E}f_{ATS}(E, B)\theta(E - E_{c1}) \\ &= g_{2LS}(E) + g_{ATS}(E, B) \end{aligned} \quad (12)$$

where n_{ATS} is the ATSs' concentration, while f_{ATS} is a magnetic-field dependent dimensionless function already described in previous papers [1] and E_{c1} is a material and weakly B -dependent energy cutoff:

$$\begin{aligned} g_{ATS}(E, \varphi) &= \int \Pi_i dE_i \delta(\Sigma_j E_j) \int dD_0 \mathcal{P}_{3LS}^*(\{E_k\}, D_0) \delta(E - \Delta\mathcal{E}) \\ &= \begin{cases} \frac{2\pi P^*}{E} \ln \left(\frac{D_{0max}}{D_{0min}} \sqrt{\frac{E^2 - D_{0min}^2 \varphi^2}{E^2 - D_{0max}^2 \varphi^2}} \right) & \text{if } E > E_{c2} \\ \frac{2\pi P^*}{E} \ln \frac{\sqrt{(E^2 - D_{0min}^2 \varphi^2)(E^2 - D_{min}^2)}}{D_{0min} D_{min} \varphi} & \text{if } E_{c1} \leq E \leq E_{c2} \\ 0 & \text{if } E < E_{c1}. \end{cases} \end{aligned} \quad (13)$$

Moreover, after an irrelevant renormalization of parameters: $E_{c1} = \sqrt{D_{min}^2 + D_{0min}^2 \varphi^2}$, $E_{c2} = \sqrt{D_{min}^2 + D_{0max}^2 \varphi^2}$, D_{min} , D_{0min} and D_{0max} being suitable (material parameters) cutoffs. A more microscopic model does not exist, at present. The gross $1/E$ dependence of the ATS DOS is one consequence of the chosen tunneling parameters' distribution, Eq. (10), and it gives rise to a peak in g_{tot} near E_{c2} that is rapidly eroded away as soon as a (weak, depending on material parameters) magnetic field is switched on. The form and evolution of the magnetic part of the DOS is shown in Fig. 8 for some chosen parameters and as a function of $\varphi \propto B$ for different values of the ATS energy gap E . This behaviour of the DOS with B is essentially the underlying mechanism for all of the experimentally observed magnetic-field effects in the studied cold glasses within this model: the measured physical properties turn out to be convolutions of this DOS (with some appropriate B -independent functions) and in turn they reproduce the shape of this DOS as functions of B (see also Fig. 17). We remark that already at $B = 0$ the TS total DOS $g_{tot}(E)$ that is here advocated, Eq. (12) above (see also Fig. 7, has the correct qualitative form that was solicited by Yu and Leggett [40] in order to achieve a better qualitative explanation for many experiments at low temperatures in the real glasses. Namely, a broad constant (due to the majority 2LSs), surmounted by a triangular-shaped contribution in a range of energy E (this part, coming from the minority ATSs). This shape is now being to a large extent justified by our model and indeed explains experimental data rather well.

3 The Magnetic Field Effects (Multi-silicate Glasses only)

We now come to the main theme for this article, the crucial piece of new experimental evidence for the cellular, RER-based scenario for glass structure. As mentioned in the Introduction, a large number of magnetic-field dependent effects have been reported in the late 1990s and early 2000s for several insulating glasses and that could not be ascribed to the (ubiquitous) trace paramagnetic impurities. We refer the reader to a review article of this Author's work so far [41], here we just review the main results that have been obtained through the proposed cellular approach and ETM low-temperature model in order to explain all such magnetic effects.

3.1 The Magnetic Field Dependent Specific Heat

Though unrecognized by the experimentalists, the heat capacity measured in some multi-component silicate glasses (pure, mono-component silica does not display such effect) has shown a strong dependence on the applied magnetic field. Such dependence was the first to be explained by the present approach [1, 42]. The total TS heat capacity is easily evaluated for this model (ETM) and obtained from the above calculated DOS

$$C_{pTS}(T, B) = \int_0^\infty dE g_{tot}(E, B) C_{p0}(E, T) \quad (14)$$

where

$$C_{p0}(E, T) = k_B \left(\frac{E}{2k_B T} \right)^2 \cosh^{-2} \left(\frac{E}{2k_B T} \right) \quad (15)$$

is the heat capacity contribution from each single TS having energy gap E and where $g_{tot}(E, B)$ is given by Eq. (12). We have made use the resulting expression to the available data [43] that display a magnetic effect

in the heat capacity in the case of two multi-component silicate glasses: commercial borosilicate Duran (from Schott GmbH) and barium-allumo-silicate (AlBaSiO, or BAS in short) glass (from Heraeus GmbH), in order to show that the ATS-ETM model works well for the magnetic-field dependent C_p . In order to fit the data, the standard phonon (T^3) contribution as well as the Langevin-paramagnetism contribution from the trace iron impurities [mostly Fe^{2+} as it turns out] need to be added to the said tunneling contributions.

The best fit for the available data is reported in Fig. 9(a) in the case of BAS glass. The concentrations of

BAS glass	Concentration [g^{-1}]	Concentration [ppm]
$n_{\text{Fe}^{2+}}$	1.06×10^{17}	14.23
$n_{\text{Fe}^{3+}}$	5.00×10^{16}	6.69
P^*n_{ATS}	5.19×10^{16}	-

Table 1: Extracted parameters (from the specific heat data [43]) for the concentrations of ATSs and Fe-impurities for the BAS glass.

Temperature [K]	D_{\min} [K]	$D_{0\min} \left \frac{q}{e} \right S$ [$\text{K}\text{\AA}^2$]	$D_{0\max} \left \frac{q}{e} \right S$ [$\text{K}\text{\AA}^2$]
0.60	0.49	4.77×10^4	3.09×10^5
0.90	0.53	5.07×10^4	2.90×10^5
1.36	0.55	5.95×10^4	2.61×10^5

Table 2: Extracted tunneling parameters (from the C_p data [43]) for the BAS glass.

the ATSs and Fe-impurities extracted from the best fit of the heat capacity data [43] as a function of B , for Duran, are reported in Table 3; having fixed the concentrations, it is then possible to extract the remaining parameters for Duran (Table 4). The fit of the available data [43] is reported in Fig. 9(b) for Duran.

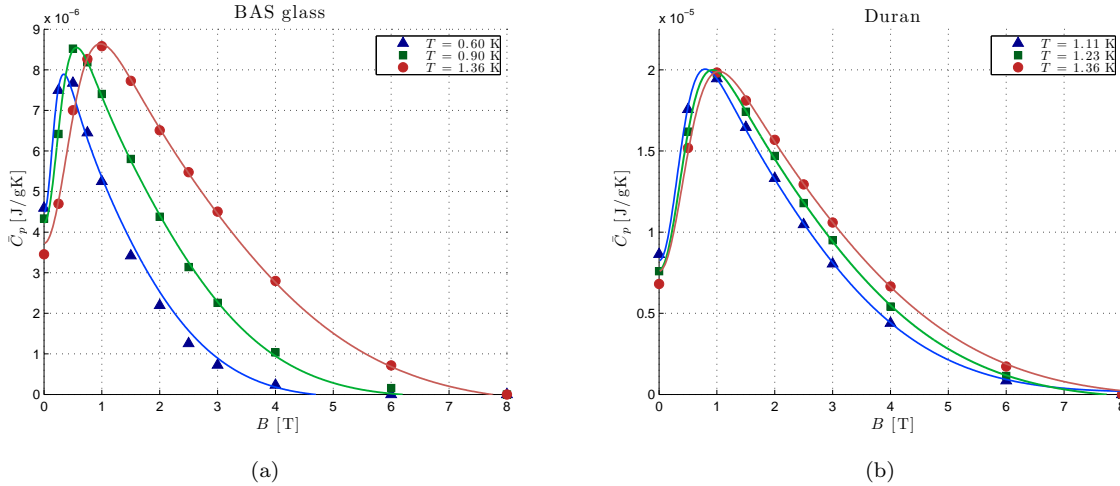


Figure 9: The heat capacity best fit for the a) BAS (or AlBaSiO) and b) Duran glasses. The continuous lines are the predictions from the ETM. Data from Ref. [43].

The results of our repeated [1] C_p analysis definitely indicate that the magnetic-field sensitive ATSs give a significant contribution to the low temperature heat capacity data. The explanation of these data [1] was the first test of the ETM and gave the first indication that the cellular structure of glass has a manifestation in experiments outside the traditional X-ray scattering domain of investigation.

3.2 The Magnetic Field Dependent Dielectric Constant

As it turns out, historically the magnetic effect on the dielectric properties of the multi-silicate glasses was the first to be discovered [9]. Only the present approach - at the time of writing - is able to explain the data,

Duran	Concentration [g ⁻¹]	Concentration [ppm]
$n_{Fe^{2+}}$	3.21×10^{17}	33.01
$n_{Fe^{3+}}$	2.11×10^{17}	21.63
$P^* n_{ATS}$	8.88×10^{16}	-

Table 3: Extracted parameters (from the heat capacity data [43]) for the concentration of ATs and Fe-impurities for Duran.

Temperature [K]	D_{min} [K]	$D_{0min} \frac{q}{e} S [\text{K}\text{\AA}^2]$	$D_{0max} \frac{q}{e} S [\text{K}\text{\AA}^2]$
1.11	0.34	4.99×10^4	2.68×10^5
1.23	0.32	5.30×10^4	2.50×10^5
1.36	0.32	5.54×10^4	2.46×10^5

Table 4: Extracted tunneling parameters (from the C_p data [43]) for Duran.

qualitatively [38] and then quantitatively [39]. We consider the contribution to the dielectric constant $\epsilon(\omega)$ from the TWPs (or ATs) that are sitting in the interstices between the RERs. One can then treat each ATS again as an *effective* 2LS having first energy gap $\Delta\mathcal{E} = \mathcal{E}_1 - \mathcal{E}_0 = E = \sqrt{D^2 + D_0^2\varphi^2}$ for relatively weak fields. Within this simplified picture, the linear-response, quasi-static resonant and relaxational contributions to the polarizability tensor $\alpha_{\mu\nu}$ can be extracted according to the general 2LS approach described in various papers [44], as well as in the review in Ref. [41], to obtain

$$\alpha_{\mu\nu}^{RES} = \int_0^\infty \frac{dE}{2E} \mathcal{G}_{\mu\nu} \left(\left\{ \frac{E_i}{E} \right\}; \mathbf{p}_i \right) \tanh \left(\frac{E}{2k_B T} \right) \delta(E - \Delta\mathcal{E}) \quad (16)$$

as well as

$$\alpha_{\mu\nu}^{REL} = \frac{1}{4k_B T} \int_0^\infty dE \left(\sum_{i,j=1}^3 \frac{E_i E_j}{E^2} p_{i\mu} p_{j\nu} \right) \cosh^{-2} \left(\frac{E}{2k_B T} \right) \delta(E - \Delta\mathcal{E}) \quad (17)$$

where

$$\mathcal{G}_{\mu\nu} \left(\left\{ \frac{E_i}{E} \right\}; \mathbf{p}_i \right) = \sum_{i=1}^3 p_{i\mu} p_{i\nu} - \sum_{i,j} \frac{E_i E_j}{E^2} p_{i\mu} p_{j\nu} \quad (18)$$

is a disorder correlator that makes use of the single-wells' electric dipoles $\mathbf{p}_i = q\mathbf{a}_i$ ($i = 1, 2, 3$). This expression assumes vanishing electric fields and no TS-TS interactions yet, an approximation which indeed does not realistically apply to experiments at the lowest temperatures. To keep the theory treatment simple, however, one can still make use of Eq. (16) and of the analogous one for the relaxational contribution to the polarizability. Interactions will play a role, though from estimates this should only happen around the 1 to 10 mK range. Eq. (16) must be averaged over the random energies' distribution (10) (denoted by $[\dots]_{av}$, responsible for the high sensitivity to weak fields) and also over the dipoles' orientations and strengths (denoted by $\overline{(\dots)}$). For a collection of ATS with $n_w > 2$ wells this averaging, as it turns out, presents serious difficulties and one must resort to the reasonable decoupling:

$$\overline{\mathcal{G}_{\mu\nu} \delta(E - \Delta\mathcal{E})} \simeq \overline{\mathcal{G}_{\mu\nu}} \cdot \overline{\delta(E - \Delta\mathcal{E})}, \quad (19)$$

where now $\overline{[\delta(E - \Delta\mathcal{E})]_{av}} = g_{ATS}(E, B)$ is the fully-averaged DOS. To calculate $\overline{\mathcal{G}_{\mu\nu}}$, one can begin by envisaging a fully-isotropic distribution of planar n_w -polygons to then obtain:

$$\overline{\mathcal{G}_{\mu\nu}} = \frac{1}{3} \left(\frac{n_w}{n_w - 1} \right) \overline{p_i^2} \frac{(n_w - 2)E^2 + D_0^2\varphi^2}{E^2} \delta_{\mu\nu}. \quad (20)$$

The second term in the numerator of Eq. (20) gives rise, one discovers, to a peak in $\delta\epsilon/\epsilon$ as a function of B at very low fields, while the first term (which is present only if $n_w > 2$) produces a *negative* contribution to $\delta\epsilon/\epsilon$ at larger B which can dominate over the enhancement term for all values of B when $D_{0max} \gg D_{0min}$, where D_{0min} , D_{0max} correspond to material-dependent cutoffs in the distribution of ATS energy barriers (V_{0max} ,

V_{0min} respectively). Observations in Duran and BK7 indeed show a significant depression of $\epsilon'(B)$ for weak fields [10], thus presenting direct evidence for the existence of ATs carrying $n_w > 2$ in the multi-silicate glasses. Performing the averaging $[\dots]_{av}$ one then gets some analytical expressions for the polarizability. The uniform average over orientation angles θ must be performed numerically (although it was checked that a very good approximation consists in the replacement $\varphi^2 \rightarrow \frac{1}{3}\varphi^2$ for averaged expressions, which corresponds to the replacement $\overline{\cos^2\theta} \rightarrow \frac{1}{3}$).

Details of the evaluation of the dielectric constant can be found in [41] and the resulting expressions appear to describe well most experimental data and for different glasses, as is shown in Figs. 10-12 using the fitting parameters presented in the Tables 5, 6.

For the sake of clarity, the data and theoretical curves in Figs. 11 and 12 have been shifted apart vertically. The quantity x_{ATS} now refers to volume concentrations of ATs, linked to mass concentrations n_{ATS} through use of the solid's density ρ : $x_{ATS} = n_{ATS}\rho$.

Material and Temperature	$\pi x_{ATS} P^* p_1^2 / \epsilon_r \epsilon_0$	D_{min}, K	$D_{0min} \left \frac{q}{e} \right S_{\Delta}, K^2$	$D_{0max} \left \frac{q}{e} \right S_{\Delta}, K^2$
BK7 15 mK	$0.089 \cdot 10^{-5}$	0.03	$1.668 \cdot 10^5$	$4.576 \cdot 10^5$
Duran 15 mK	$0.052 \cdot 10^{-5}$	0.021	$2.457 \cdot 10^5$	$4.151 \cdot 10^5$
AlBaSiO 50 mK	$0.89 \cdot 10^{-5}$	0.015	$2.440 \cdot 10^5$	$3.080 \cdot 10^5$
AlBaSiO 94 mK	$3.75 \cdot 10^{-5}$	0.025	$1.225 \cdot 10^5$	$1.589 \cdot 10^5$
AlBaSiO 120 mK	$3.09 \cdot 10^{-5}$	0.0227	$1.767 \cdot 10^5$	$2.248 \cdot 10^5$

Table 5: Fitting parameters extracted for the dielectric constant in a magnetic field and for three different types of glasses.

Temperature	$\pi x_{ATS} P^* p_1^2 / \epsilon_r \epsilon_0$	D_{min}, K	$D_{0min} \left \frac{q}{e} \right S_{\Delta}, K^2$	$D_{0max} \left \frac{q}{e} \right S_{\Delta}, K^2$
50 mK	$4.38 \cdot 10^{-5}$	0.015	$0.076 \cdot 10^3$	$3.047 \cdot 10^4$
70 mK	$12.22 \cdot 10^{-5}$	0.0486	$0.600 \cdot 10^3$	$2.662 \cdot 10^4$
100 mK	$13.63 \cdot 10^{-5}$	0.0486	$3.035 \cdot 10^3$	$7.616 \cdot 10^4$

Table 6: Fitting parameters for the (non nuclear-quadrupole moments containing) $SiO_{2+x}C_yH_z$ glass for different temperatures.

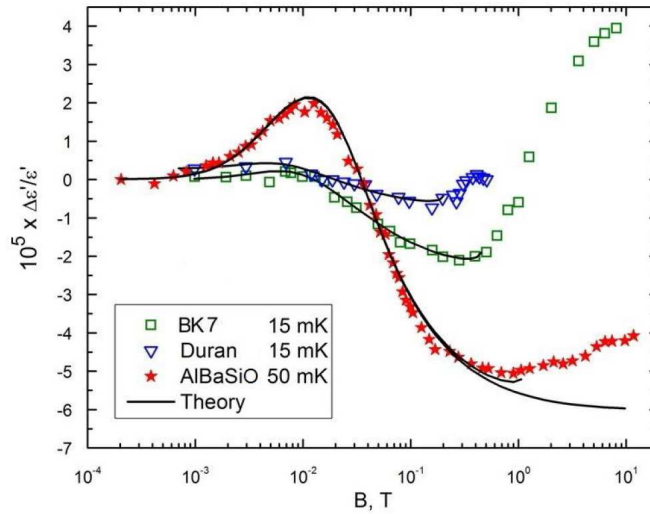


Figure 10: Relative dielectric constant variation versus the magnetic field for AlBaSiO (or BAS) [10]b, BK7 [10] and Duran [10]b glasses. With best-fit parameters given in Table 5, the continuous curves are the results of our theory in the “weak field” approximation with (and - for AlBaSiO - also without) higher order correction. From [46].

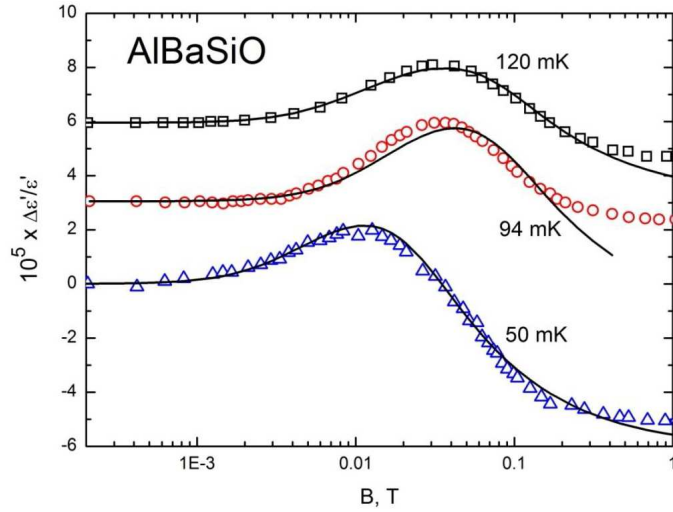


Figure 11: Relative dielectric constant variation versus the magnetic field and temperature for AlBaSiO (or BAS) glass [10]b. With fitting parameters as in Table 5, the continuous curves are the result of our theory in the “weak field” approximation. From [46].

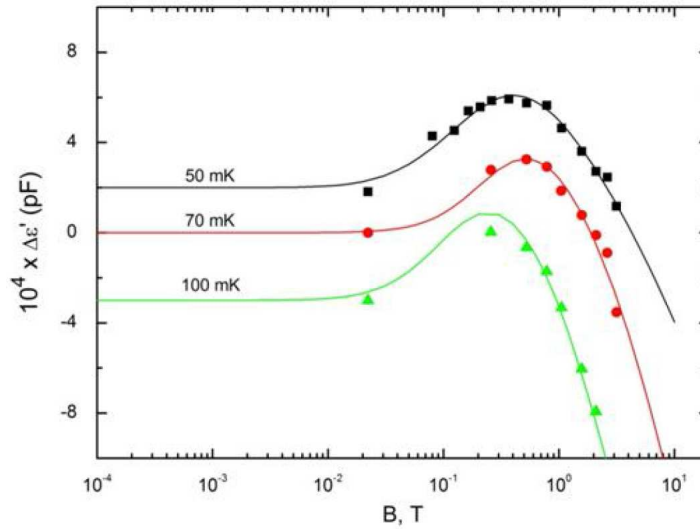


Figure 12: Dielectric constant variation as a function of the magnetic field and temperature for the (non nuclear-quadrupole moments containing) $\text{SiO}_{2+x}\text{C}_y\text{H}_z$ glass [47]. Fitting parameters as in Table 6. From [46].

Analogous results have been obtained for the explanation of the dielectric loss data in a magnetic field, the theory and fits of the available experimental data can be found in [41]. The tunneling parameters extracted from the data fitting compare well with those given above, so that in fact a single model with a single set of material parameters per specimen could be used in all these studies (except that the fit of all the data sets would not be so good). Here we only like to remark that for the loss the theory must also describe the magnetic-field dependence of a phenomenological relaxation time, a new parameter entering in the description of dielectric dissipation. This relaxation time for ATs at low temperature and in a magnetic field is now found to be given by the following expression (derived, yet no detailed published, by the present Author) [41]:

$$\tau_{ATS}^{-1} = \tau^{-1}(E, \varphi) = \frac{E^3 (D_0^2 \varphi^2 + \frac{5}{6} D^2)}{\Gamma \tanh\left(\frac{E}{2k_B T}\right)} = \frac{E^3 (E^2 - \frac{1}{6} D^2)}{\Gamma \tanh\left(\frac{E}{2k_B T}\right)} = \tau^{-1}(E, D) \quad (21)$$

where, as usual, the A-B phase φ is directly proportional to the magnetic field B . It appears, therefore, that the total dielectric relaxation time, obtained through its inverse:

$$\frac{1}{\tau_{tot}} = \frac{1}{\tau_{2LS}} + \frac{1}{\tau_{ATS}(\varphi)} \quad (22)$$

must diminish in a non-trivial manner as the magnetic field is switched on. This very interesting prediction of the present theory appears to be confirmed explicitly, albeit only qualitatively, in laboratory experiments and for some special multi-silicate glasses so far only via the work of a Russian group at liquid-He temperatures [48]. A systematic study of the magnetic-field dependence of τ_{tot} in the multi-component glasses is lamentably still lacking.

3.3 The Magnetic Field Dependent Polarization Echo Amplitude

The experimental detection of electric and phonon echoes in glasses is one strongly convincing argument for the 2LSs' existence. Echoes in glasses are similar (yet with important differences) to other echo phenomena such as nuclear spin echo, photon echo and so on. But only at very low temperatures the relaxation of the TSs becomes so slow that coherent phenomena like polarization echoes become observable in the insulating glasses [35].

The essence of the effect is as follows (see Fig. 13). A glass sample placed in a reentrant resonating cavity ("Topfkreisresonator") is subjected to two very short ac electromagnetic pulses at the nominal frequency of about 1 GHz and separated by a time interval τ_{12} . The durations τ_1 and τ_2 of the pulses must be much shorter than all relaxation process times in the observed system. The macroscopic polarization produced by the first pulse then vanishes rapidly, due to the broad distribution of parameters of the TSs in glasses. This phenomenon is similar to the well-known free-induction decay that is observed in nuclear magnetic resonance (NMR) experiments. The "phase" (energy-level populations) of each 2LS develops freely between the two exciting pulses. The second pulse causes an effective "time reversal" for the development of the phase of the 2LSs. The initial macroscopic polarization of the glass is then recovered at a time τ_{12} , roughly, after the second pulse. Because the thermal relaxation processes and (see below) spectral diffusion are strongly temperature dependent, polarization echoes in glasses can be observed, in practice, only at very low temperatures: typically below 100 mK. The echo amplitude is clearly proportional to the number of 2LSs that are in or near resonance with the exciting microwave pulse and that do not lose their phase coherence during the time $2\tau_{12}$ [35]. It should be stressed that, because of the wide distribution for the parameters of the two-level systems in glasses, the theoretical description of polarization echoes in glasses is considerably more complicated than in the case of nuclear spin systems. In analogy to the two-pulse echo in NMR experiments this phenomenon is referred to as the spontaneous electric echo.

Polarization echo phenomena can help us understand more about the microscopic structure of TSs in general in glasses and give different kinds of information. The analysis of these experiments is similar to that for the analogous NMR case, except that the TS problem is complicated by three new factors. First, the elastic (or electric) dipoles are not aligned with respect to the driving field(s) and a calculation of the echo signal involves averaging over their orientations. Second, for a given pumping frequency ω there exists a distribution of induced moments (elastic or electric) and relaxation times, which must be included in the theoretical analysis. Finally, in electric echo experiments the local field as seen by the TSs is not equal to the externally applied field, and a local-field correction factor must be used when evaluating absolute values of the polarization [35].

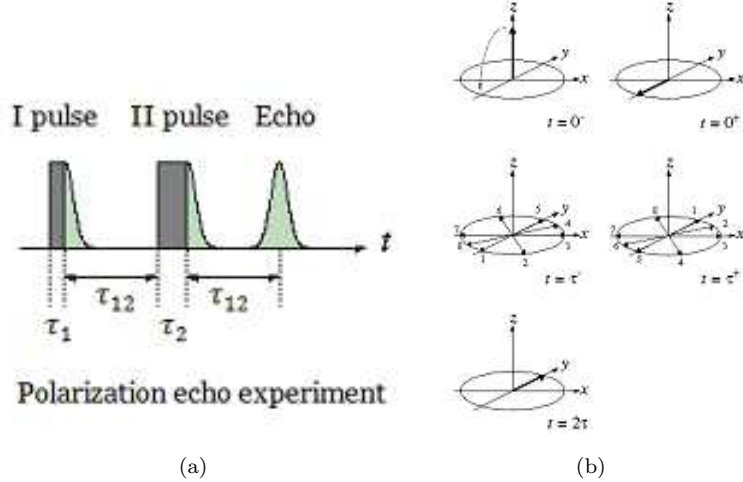


Figure 13: Schematics of the two-pulse polarization echo experiment. Hahn's vectorial interpretation on the right hand side is for NMR's spin-echo experiment.

In the polarization echo experiments, done typically at radio frequencies and at very low temperature (about 10 to 100 mK), it has been established that the TSs in glasses couple directly to the magnetic field B [45, 49]. This time, the amplitude of two-pulse echoes in the BAS, Duran and BK7 glasses was found to depend strongly on the applied magnetic field showing a non-monotonic (perhaps oscillatory) field variation and for all glass types. Since the very beginning [11, 50], such behavior was attributed to the existence of nuclear electric quadrupole moments (NEQM) carried by some of the tunneling species (having nuclear spin $I > \frac{1}{2}$) interacting via their nuclear magnetic dipole with the magnetic field and also with gradients of the internal microscopic electric field. The NEQM model is based on the consideration that the levels of tunneling particles with non-zero nuclear quadrupole moment experience a nuclear quadrupole splitting, which is different in the ground state and in the excited state of a tunneling 2LS. The magnetic field then causes an additional Zeeman splitting of these levels, giving rise to interference effects. In turn, these two different nuclear interactions, though very weak, are thought to be causing the non-monotonic magnetic field variation of the echo amplitude.

The amplitude (in fact, integrated amplitude) of two-pulse polarization echoes of four types of silicate glasses is now shown in Fig. 14(a) and as a function of the magnetic field [49]. In contrast to various other low-temperature properties of glasses, the influence of the magnetic field on the amplitude of spontaneous echoes is manifestly not universal on the qualitative level already. BK7 and Duran show similar effects, and yet the concentration of magnetic impurities differs by at least a factor of 20 (a clear indication, that such impurities are irrelevant for such effects). The most remarkable result of these measurements is the fact that Suprasil I (very pure α -SiO₂) shows no detectable magnetic-field effect. While Duran, BAS and BK7 contain nuclei with non-zero nuclear quadrupole moment, Suprasil I is virtually free of such nuclei, except for a tiny % of ¹⁷O. This fact has been used to provide the justification for the nuclear quadrupole theory. The variation of the echo amplitude with the applied magnetic field is similar for Duran, BK7 and BAS, but not at all qualitatively identical. All three samples exhibit a marked principal maximum at very weak fields, $B \sim 10$ mT, but only BK7 has a relevant second maximum and some hint to an oscillation as a function of B . Unexplained by the NEQM theory, the high fields the amplitude of the echo rises well above its value at zero magnetic field and seemingly saturates (yet, see Figs. 9 and 17 below, this is very similar to what happens to the inverted heat capacity, $-C_p$, as a function of B). Again unexplained by NEQM theory, there is a piece of linear dependence on B at intermediate fields.

In Figure 14(b) the amplitude of spontaneous echoes for the BK7 glass is reproduced as a function of the applied magnetic field and for different delay times τ_{12} between the exciting pulses. We can see some obvious qualitative differences for different values of τ_{12} and that a second maximum (the "oscillation") is not always present. These findings necessitate a good theory for spectral diffusion [51] in real glasses (containing both 2LSs and ATSS) and this theory remains to date unaccomplished.

One of the most remarkable facts about the experiments on echoes from glasses in a weak magnetic field is that strong magnetic response is not confined to the inorganic, multi-silicate glasses. The amplitude of

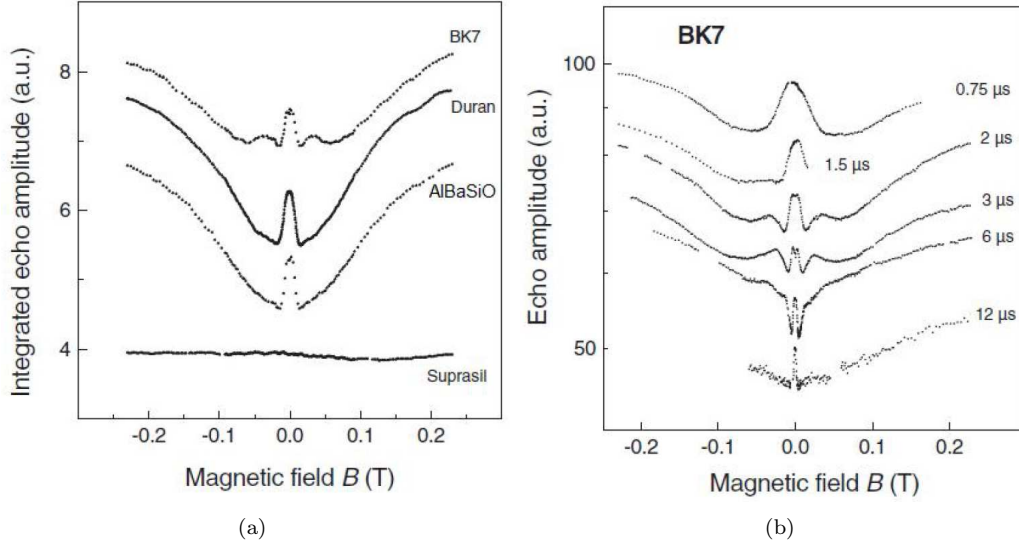


Figure 14: Data from [45] a) The integrated echo amplitude plotted as a function of the magnetic field for different silicate glasses: BK7, Duran, AlBaSiO (BAS) and Suprasil I. All data were taken at $T=12$ mK, $\tau_{12}=2 \mu$ s, and nominally 1 GHz, except for Duran, where the delay time was $\tau_{12}=1.7 \mu$ s. b) The amplitude of two-pulse echoes in BK7 glass vs. the magnetic field for different values of the waiting time τ_{12} between pulses. All data sets were taken at 4.6 GHz and 12 mK except that for $\tau_{12}=2 \mu$ s which was taken at 0.9 GHz (this behaviour, right panel, remains unexplained by all existing theories and a real challenge).

spontaneous echoes in part-deuterated and in undeuterated amorphous glycerol as a function of the weak magnetic field B has been demonstrated to show completely different behaviour [11]. In the case of ordinary glycerol there is some, very small change of the echo amplitude with B . However, for partially deuterated glycerol the change is considerably more noticeable, of different shapes and duration. These experiments *seemingly* provide proof that the magnetic effects are of nuclear origin, since the two amorphous glycerol samples differ only in the content of nuclei carrying a NEQM. As it turns out, a comparative analysis of experiments in different isotope-concentration samples hints to the fact that the effect does not scale at all with NEQM concentration. The explanation of the magnetic effects in amorphous glycerol echo experiments goes beyond the aims of this review and an explanation based on the ETM can be found in the review [41] and first published in [39]. The vitreous-glycerol experiments show, however, that the tunneling species are H^+ and/or D^+ in these samples: correctly, the lighter atomic species. Then, in the multi-silicates the tunneling particles ought to be overwhelmingly O^{2-} , hardly the NEQM-carrying B^{3+} , Na^+ , K^+ , or Al^{3+} as claimed by NEQM-theory supporters. The status of the NEQM-theory remains unclear.

We will discuss in this essay principally the echo experiments on the silicates. A theory for the echo signal from a collection of 2LSs can be obtained - and from first principles - from a lengthy but straightforward Schrödinger equation (or density matrix) treatment in which high-frequency modes are neglected and the phonon-damping is treated in a phenomenological way [46]. In the more rigorous way, we have obtained for the echo signal an expression which confirms and in fact improves on the theory of 2LSs' electric echoes by [52] [some details can also be found in [41]]. It is then possible to extend this polarization echo's calculation to the case of the ATS-ETM describing glasses in a magnetic field [46, 39]. The point of view is taken that a background of ordinary 2LSs - insensitive to the magnetic field - also exists in the glass, but is not needed in order to explain the data as a function of the magnetic field.

One begins with a collection of 3LSs (now $n_w = 3$ is not just computationally convenient, but physically correct as explained in Section 2), but with each single ATS Hamiltonian written in the (diagonal) energy representation:

$$H' = SHS^{-1} = \begin{pmatrix} \mathcal{E}_0 & 0 & 0 \\ 0 & \mathcal{E}_1 & 0 \\ 0 & 0 & \mathcal{E}_2 \end{pmatrix} + S \begin{pmatrix} -\mathbf{p}_1 \cdot \mathbf{F} & 0 & 0 \\ 0 & -\mathbf{p}_2 \cdot \mathbf{F} & 0 \\ 0 & 0 & -\mathbf{p}_3 \cdot \mathbf{F} \end{pmatrix} S^{-1} \quad (23)$$

Here the transformation matrix $S = S(\varphi)$ is magnetic-field dependent, the \mathcal{E}_i are the (B -dependent) ATS

energy levels and the \mathbf{p}_i are the single wells' electric dipoles. As in the treatment of Gurevich *et al.* [52] there is also a phonon bath and this will be treated - as usual - phenomenologically and resulting in a standard phonon-damping exponential. The second term in Eq. (23) causes irrelevant energy-level shifts and also produces an extra matrix term $\Delta H'(t) = (A_{ij})$ of which the only relevant element is of the form

$$A_{01} = A_{10}^* = \sum_{k=1}^3 -\mathbf{p}_k \cdot \mathbf{F}_0 S_{0k}(\varphi) S_{1k}^*(\varphi) \cos \omega t \quad (24)$$

These A_{ij} cause quantum transitions between the ATS levels ($|0\rangle, |1\rangle, |2\rangle$) when the electric-field pulses are applied. In the weak magnetic field limit (now most appropriate for these experiments) and in the usual approximation $D \ll D_0$ (which is always consistent with our best fits to the data), one discovers that the second excited level $|2\rangle$ remains unperturbed and one can make use of the effective 2LS approximation (where, however, the ground-state single-well wavefunctions mix). One can then repeat the Schrödinger equation (or density-matrix) calculation carried out for the 2LS case, introducing though the complex Rabi frequency:

$$\Omega_0 = \frac{A_{01}}{\hbar} \quad (25)$$

The evolution of the generic ATS during, or in the absence, of pulses then gets to be followed exactly in much the same way as before, except that in order to simplify the formalism it is convenient to introduce right from the beginning the orientationally-averaged Rabi frequency (which is now a real quantity):

$$\Omega_R = \sqrt{|\Omega_0|^2} \quad (26)$$

the bar denoting averaging over the 3LS base-triangle's orientation. Replacing Ω_0 with Ω_R before carrying out this averaging of the sample's polarization is here our main approximation, allowing for a considerably simplified treatment and leading to the following magnetic-field dependent Rabi frequency:

$$\Omega_R = \frac{p_1 F_0}{\hbar} \sqrt{\frac{D_0^2 \varphi^2 + \frac{5}{6} D^2}{6E^2}} \quad (27)$$

Here, \mathbf{p}_1 is the single-well (orientation-averaged) electric dipole and $E = \hbar\omega_0 = \sqrt{D^2 + D_0^2 \varphi^2}$ is the usual magnetic-field dependent lower energy gap, in the weak field and near-degenerate approximations. The above form for Ω_0 of course treats incorrectly the ATSs that have \mathbf{F}_0 roughly orthogonal to the ATS base triangle; fortunately these have $\Omega_0 \approx 0$ and in fact do not contribute to the echo signal.

Proceeding as in our own derivation of the ordinary 2LSs echo [46], one finds that there is indeed a magnetic contribution to the polarization of the sample from the generic ATS and (partly averaged) given by:

$$\begin{aligned} \Delta \wp_{\parallel}(t) \cong & -\frac{\hbar}{F_0} \tanh\left(\frac{E}{2k_B T}\right) e^{-\frac{\gamma}{2}t} \frac{\Omega_R^4}{\Omega_G^3} \\ & \text{Im} \left\{ \sin^2\left(\frac{\Omega_G \tau_2}{2}\right) \left[\sin(\Omega_G \tau_1) - 2i \frac{\omega_0 - \omega}{\Omega_R} \sin^2\left(\frac{\Omega_G \tau_1}{2}\right) \right] \right\} e^{i\Phi(t) - i \int_0^t \Delta\omega(t') s(t') dt'} \end{aligned} \quad (28)$$

Here, $\frac{\gamma}{2} = \tau^{-1}$ is the magnetic ATS relaxation rate due to phonons and given by Eq. (21), so the generalized Rabi frequency is still given by $\Omega_G = \sqrt{\Omega_R^2 + (\omega_0 - \omega)^2}$ and, moreover:

$$\Phi(t) = \omega_0(t - 2\bar{\tau}_{12}) + \omega \Delta\tau \quad (29)$$

is what we find to be the appropriate time argument. From this, it is obvious that the time at which all the ATSs (regardless of energy gap $E = \hbar\omega_0$ value) get to be refocused is $t = 2\bar{\tau}_{12}$ and this determines the correct echo's peak position (when the echo signal has a reasonable shape, this not being always the case [45]). The measured echo amplitude's contribution from the magnetic ATS is then (also allowing for an arbitrary amplification factor A_0):

$$\begin{aligned} \Delta A(\varphi) = & A_0 \frac{d}{\varepsilon_0 \varepsilon_r} x_{ATS} 2\pi P^* \int_0^\infty dE \int \frac{dD}{D} \int \frac{dD_0}{D_0} \Theta(D, D_0) \\ & \times \delta\left(E - \sqrt{D^2 + D_0^2 \varphi^2}\right) \Delta \wp_{\parallel}(2\bar{\tau}_{12}) \end{aligned} \quad (30)$$

where now d is the sample's thickness, $\Theta(D, D_0)$ is a Dirichlet's theta-function restriction for the integration domain (see [46]) and where a final orientational-averaging with respect to the angle (defining the A-B phase φ , see Eq. (7)) $\beta = \widehat{\mathbf{BS}}_\Delta$ is in order. One deals with the delta-function's constraint and the energy parameters' integrations in the usual way to arrive at, after a lengthy calculation:

$$\begin{aligned} \Delta A(\varphi) \cong & -A_0 \frac{d}{\varepsilon_0 \varepsilon_r} x_{ATS} \frac{4\pi \hbar^2 P^*}{F_0} \cos(\omega \Delta \tau) \\ & \times \int_{E_{c_1}}^{E_{c_2}} \frac{dE}{E} \int_{D_{min}}^{D_2(\varphi)} \frac{dD}{D} \tanh\left(\frac{E}{2k_B T}\right) \frac{E^2}{E^2 - D^2} \\ & \cdot e^{-w_{27} \tau_{12}} \Omega_R^2 \sigma(E) [S(\theta_1, \theta_2) \tan(\omega \Delta \tau) + C(\theta_1, \theta_2)] \\ & + \int_{E_{c_2}}^{\infty} \frac{dE}{E} \int_{D_1(\varphi)}^{D_2(\varphi)} \frac{dD}{D} (\text{same integrand as above} \dots) \end{aligned} \quad (31)$$

where we have defined the special functions:

$$\begin{aligned} \sigma(E) &= \frac{\Omega_R^2}{2\hbar \Omega_G^3} = \frac{\Omega_R^2}{2\hbar (\Omega_R^2 + (\omega_0 - \omega)^2)^{3/2}} \\ S(\theta_1, \theta_2) &= \sin(\Omega_G \tau_1) \sin^2(\Omega_G \tau_2 / 2) \\ C(\theta_1, \theta_2) &= -2 \frac{\omega_0 - \omega}{\Omega_R} \sin^2(\Omega_G \tau_1 / 2) \sin^2(\Omega_G \tau_2 / 2) \end{aligned} \quad (32)$$

and where $\theta_{1,2} = \Omega_G \tau_{1,2}$ are the so-called pulse areas. $E_{c_{1,2}}$ are as in the previous Sections whilst now: $D_{1,2}(\varphi) = \sqrt{E^2 - D_{0max,min}^2 \varphi^2}$ and $E = \hbar \omega_0$.

In going from Eq. (28) to Eq. (31) we have tacitly made some assumptions on the (to be fully averaged) spectral diffusion term, $e^{-i \int_0^{\tau_{12}} \Delta \omega(t') s(t') dt'}$ (where $\hbar \Delta \omega(t) = E(t) - E$ represents the time fluctuation of the ATS's energy gap which is due to local strain and/or electric field fluctuations [51]). The theory of spectral diffusion (SD) [51] for the ATSS is still to be accomplished, but we can safely assume that what was found by many Authors for NMR's spin-echoes as well as for the 2LS polarization echoes in glasses holds good for the ATSS too. Namely: there is a wide range of waiting times τ_{12} values where the decay of the echo amplitude well approximates a simple exponential form, so that one can replace the SD term with $e^{-2\tau_{12}/\tau_\phi}$, $\tau_\phi(T)$ being a SD characteristic time depending only on temperature. There should be a SD time $\tau_{\phi(3)}$ for the ATSS just like there is a SD time $\tau_{\phi(2)}$ for the standard 2LSs' ensemble. For the latter, STM theory has shown [53, 51] that the latter parameter is independent of E and thus for the ATS we shall assume the very same and, moreover, that (just as for the phonon damping rate and for Rabi frequency) its own dependence on B is weak or absent. This allows us to lump the SD problem together with phonon damping, yielding - in essence - an overall exponential relaxation rate:

$$w(E, D) = \tau_\phi^{-1} + \tau^{-1}(E, D) \quad (33)$$

where the SD-time $\tau_{\phi(3)}$ is typically much shorter than the phonon-damping time τ and depends on temperature only, through:

$$\tau_{\phi(3)}^{-1} = c_{ATS} T \quad (34)$$

where c_{ATS} is an appropriate constant. The assumption of an overall simple-exponential decay of the echo amplitude with waiting time τ_{12} and characteristic time $\tau_{\phi(2)} = 1/c_{2LS} T$ seems to be well verified experimentally [54] for single-component glasses (uncontaminated a-B₂O₃, a-SiO₂ etc.). Clearly, a better theory for SD in multi-component glasses is however in order.

We now make use of Eq. (31) to fit some of the available experimental data for the multi-silicates, the idea being that the total amplitude is given by a sovraposition of 2LS and ATS contributions: $A(\varphi) = A_{2LS} + \Delta A(\varphi)$ (which must still be averaged with respect to the ATS magnetic-orientation angle β). Fig. 15 shows the experimental results for the *relative* echo amplitude in AlBaSiO (or BAS glass) as a function of B . Values of B up to 0.6 T have been explored, and for three distinct temperatures. The data are then fitted with our theory (full curves) with the parameters reported in Table 7. The agreement between theory and experiment is indeed highly satisfactory, given the discussed simplifications and assumptions that

have been used in the theory. Only one minimum in $A(B)$ is found and the inset in Fig. 15 shows that, again, it is the ATS magnetic DOS that is causing the magnetic effect (Section 3). In fact, by enforcing the strict-resonance condition $\sigma(E) \rightarrow \delta(E - \hbar\omega)$ Eq. (31) would collapse to a quantity very much like the DOS (convoluted with slow-varying, in E , corrections) and with the very same DOS behaviour, reproducing in this way the qualitative shape of $\Delta A(B)$. It is however the non-resonant convolution of this quasi-DOS with other (smooth) E -dependent functions that produces the rounding of the minimum in $\Delta A(B)$ and the B^{-2} saturation that is always observed. Interestingly enough, now τ (though $\tau_\phi \ll \tau$) the phonon-damping term plays a main role in the rounding of the high- B tail of $\Delta A(B)$ to the B^{-2} (as observed) saturation. The ATS approach is the only theory that predicts also a linear-in- B intermediate decay regime of the echo amplitude, and this is often experimentally observed. Details of the ETM theory for the electric echo are interesting and will be published elsewhere. Next, in Fig. 16 we produce the comparison of theory and experiment for data

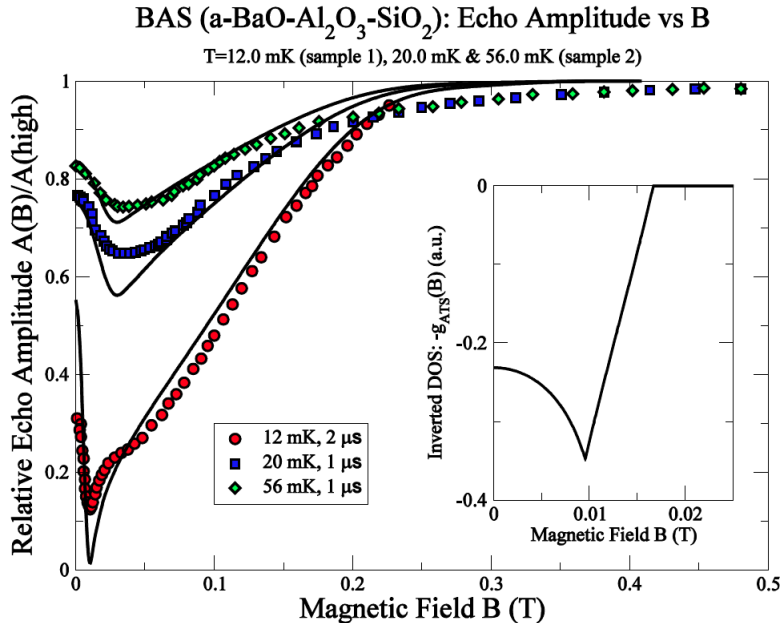


Figure 15: Magnetic field dependence of the polarization echo *relative* amplitude (relative to its value at “high” fields, where saturation occurs) for the AlBaSiO glass [49] (also referred to as BAS glass) at given experimental conditions. We believe that two separate samples have been used. The continuous curves are from our theory. Nominal frequency 1 GHz, $\tau_2 = 2\tau_1 = 0.2 \mu\text{s}$. Inset: behaviour of the ATS DOS for the same parameters (this is the physical origin of the effect).

for the echo amplitude in BK7 (this is good optical glass, hence devoid of true microcrystals, but nevertheless containing the (large) RERs) at two different values of the waiting time τ_{12} . It is truly remarkable how our ETM theory, despite the many simplifications and assumptions and the total absence of multi-level quantum physics (as advocated by the NEQM approach), can reproduce all the features qualitatively characterizing the experimental data, including every change in curvature of $A(B)$ vs. B . A preliminary rough fit, reported, not aiming at high χ^2 agreement, reproduces also two maxima (and minima) that the NEQM approach takes as indication of the multiple (rapid) oscillations ensuing from the quantum beatings ascribed to the Zeeman- and NEQM-splitting of the generic 2LS [50] and NEQM-carrying tunneling particle. There are in fact never more than two observed minima, in the experimental data, and these can be reproduced by the present, simpler ATS-ETM approach. Finally, in the inset of Fig. 16 we show what the experimentalists overlooked, by not exploring higher magnetic-field values. Using a simple-minded low- φ correction for the lower energy gap at higher fields, we plot the expected behaviour of $A(B)$ for intermediate fields. After the two observed minima, there is only an apparent saturation, yet new interesting features ought to characterise $A(B)$ at higher fields ($B > 600$ mT). This, just as it happens for the dielectric constant (Section 5). A full description of the high field effects, however, requires a calculation involving all three ATS energy levels (this was never done).

This concludes this very short survey of the main results obtained within the ETM model for the low-

BK7: Echo Amplitude vs B (T=12 mK)

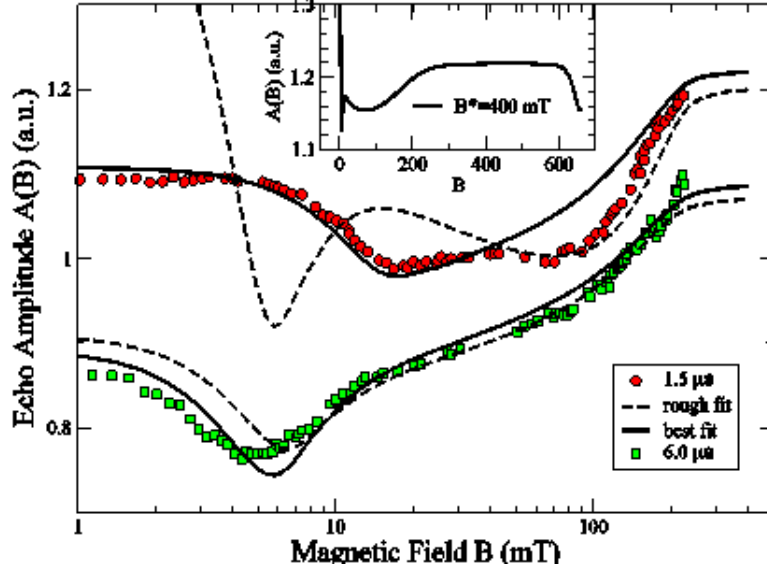


Figure 16: Magnetic-field dependence of the polarization echo amplitude for borosilicate BK7 glass [49] at given experimental conditions. Dashed curves (preliminary rough fit) and continuous curves from our theory: there are no more than two observable maxima or minima (so, no true oscillations). Nominal frequency 0.9 GHz, $\tau_2 = 2\tau_1 = 0.2 \mu\text{s}$. Inset: our prediction for the higher magnetic field regime (B^* as defined in Section 5, Ref. [41]).

Glass type	D_{min} (mK)	$D_{0min} \left \frac{q}{e} \right S_{\Delta}$ ($\text{K}\text{\AA}^2$)	$D_{0max} \left \frac{q}{e} \right S_{\Delta}$ ($\text{K}\text{\AA}^2$)	Γ^{-1} (μsK^5) $^{-1}$	$c_{ATS} - c_{2LS}$ (μsK) $^{-1}$	$p_1 F_0$ D kV m^{-1}	$\tan \omega \Delta \tau$
AlBaSiO (sample 1)	17.74	0.95×10^3	2.13×10^4	9.22×10^6	5.008	0.461	0.247
AlBaSiO (sample 2)	27.20	1.14×10^3	8.96×10^3	2.57×10^5	3.825	0.450	0.245
BK7 (1.5 μs)	16.76	0.92×10^3	1.34×10^4	8.91×10^6	1.03 (*)	0.60	0.207
BK7 (6 μs)	15.94	0.89×10^3	3.31×10^4	3.25×10^6	5.72 (*)	0.98	0.204

Table 7: Fitting parameters for the echo amplitude’s magnetic-field dependence. (*) For BK7 (best-fit parameters only), only c_{ATS} is involved.

temperature magnetic-field effects. The treatment shows that all the magnetic effects (basically: an enhancement at low fields, followed by a decrease in each probed quantity at the higher fields) appear to be the consequences of the very same magnetic behaviour of the ATS DOS (described in Section 2). In Fig. 17 we have re-drawn the magnetic-field dependence of the relative dielectric constant's change and (different scale) of the *inverted* relative echo amplitude variation. The variation of the heat capacity C_p has not been inserted for clarity, nevertheless it follows exactly the very same trend as for $-A(B)/A(\text{high})$ (see Figs. 9(a) and (b)). The schematic change of the ATS DOS, $g_{ATS}(B)$ is also shown (not to scale) and it appears to determine the trend observed in all three experiments.

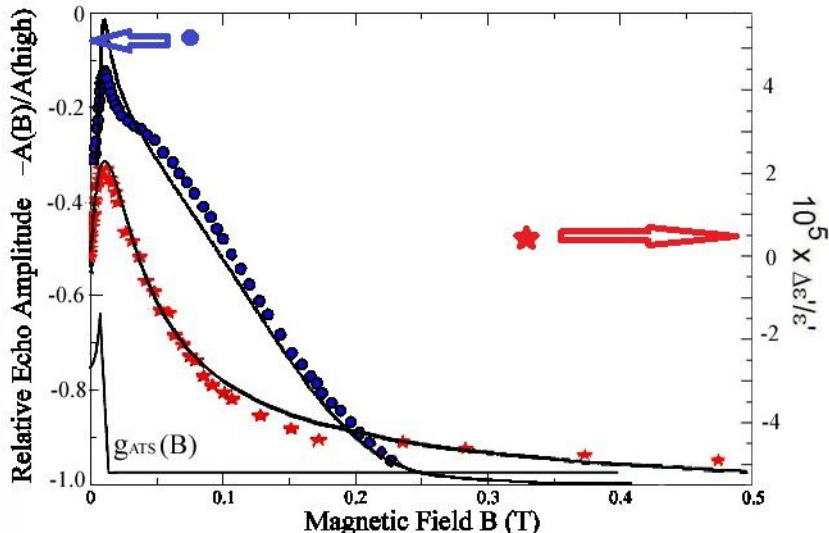


Figure 17: Some data (for the same glass type, BAS) showing the magnetic-field variation of (minus) the echo amplitude $-A(B)/A(\text{high})$ (blue dots) and of the dielectric constant variation (different scale, red stars). The qualitative variation (which mimicks that of the heat capacity C_p , see Figs. 9(a) and (b)) derives from that of the magnetic DOS, $g_{ATS}(B)$, drawn not to scale. The black lines are all theory predictions.

4 Consequences, Conclusions and Outlook

4.1 A new scenario for the glass transition?

Having conceived a heterogeneously disordered, cellular make-up of the glassy state, it seems natural to ask what the implications for the onset of the glassy state would be. The crucial question is the definition of the glass transition, which can only be kinetic in nature given the continuity that is being advocated between the dynamical heterogeneities of the supercooled state and those of the glassy state. Namely, it is envisaged that the better-ordered regions, or RERs or solid-like clusters in the supercooled state grow in size with decreasing temperature till a limit size ξ_0 is reached. Thereafter a mutually hindering state sets in for the maximally grown RERs and they must grow through a completely different (and much slower) mechanism for consolidation to take place at the expense of the material (if any) in the interstitial spaces. Naively we can take the temperature where ξ_0 is attained as the glass transition temperature T_g . At this temperature the substance is made up of close-packed RERs of maximum size ξ_0 which are better ordered, though not crystalline, and - depending on composition - of fluid-like atomic species in the interstitial spaces (or cages) between the RERs. The true crystals have not had the chance to grow, either because kinetically disfavoured

or because their size does not allow for true order (thus RERs have formed instead). The time necessary for the coalescence and grow of true crystals has not been made available in the quench.

We can describe the dependence of T_g , the temperature where the polycluster forms, on the cooling rate κ by envisaging a characteristic microscopic time τ_0 for the cells' rearrangement and an entropy (per atomic species) for the many ways the polycluster can be formed from the cooperative nucleation of such cells:

$$s(T) = k_B \ln \left[\frac{T_c - T}{\kappa \tau_0} \right] \quad (35)$$

much in the same spirit as in Adam-Gibbs' treatment for the onset of the glassy state [18]. On dimensional grounds, and treating this entropy as a response susceptibility for the glass transition, one then writes (if w_0 is a characteristic energy, per atomic species, for the polycluster formation):

$$s(T_g) = k_B \ln \left[\frac{T_c - T_g}{\kappa \tau_0} \right] = \frac{w_0}{T_g} \quad (36)$$

If the written form of the above susceptibility is regarded as a Curie-like approximation in which the nucleating cells are not yet interacting, then the molecular-field improved form of the Curie-Weiss type would lead us to write

$$k_B \ln \left[\frac{T_c - T_g}{\kappa \tau_0} \right] = \frac{w_0}{T_g - \Theta} \quad (37)$$

where Θ is a characteristic temperature below T_g that takes nucleating cell-cell interactions into account. A graphical study of the above Eq. (37) for $T_g(\kappa)$ shows that T_g increases logarithmically with κ , as is known experimentally (see e.g. [57]) and from computer simulations (see e.g. [58]). A full derivation from nucleation theory of the above reasoning will be reported elsewhere.

4.2 Some conclusions from the magnetic effects: estimate of cell size

Qualitatively at least, our cellular-structure based ETM explains all low-temperature experimental observations so far [for a more complete discussion see [41]]. Looking at the parameters which have been used for the best fits, one cannot fail to recognize (see e.g. Table 7) that for the echo experiments the extracted values of the cutoffs for the parameter combinations $D_0 \frac{q}{e} S_\Delta$ are approximately one order of magnitude smaller than those used for the other experiments, namely for C_p and ϵ . The latter have been carried out inside higher temperature ranges, as it turns out. This could be explained through a mechanism where the number of elementary atomic tunneling systems N within each single one ATS (hence inside each interstice, or cage, between the RERs or mosaic cells or grains) gets to be characterised by a temperature dependence $N(T) = N_0 \exp\{-E_0/(k_B T)\}$. Namely: there is a consolidation mechanism especially important at the lowest temperatures where ions from the interstices get to be absorbed in the cells (see Fig. 3) and the resulting number of coherently tunneling particles making up each ATS diminishes with diminishing temperature. We have conducted an analysis of the paramagnetic magnetization of samples of Duran, BAS and BK7 glass reported in the literature as a function of temperature using the idea of the cell model and ATS tunneling in the interstices with a temperature-dependent $N(T)$ [42]. We have obtained in this way good fits to the data and an estimate of the Fe impurity concentrations that are in agreement with the concentrations extracted from the low-temperature C_p data (Tables 1 and 3). The number N of coherently tunneling ions making up each ATS then enters the parameter combination $D_0 \frac{q}{e} S_\Delta$ as $[N(T)]^3$ times a combination of factors specific for a single atomic tunneling particle and the T -dependence of the extracted combination of cutoff and other tunneling parameters receives its rationale. Though it might seem surprising that the tunneling parameter D_0 of a collection of N coherently tunneling atomic particles gets to scale like N times a microscopic tunneling parameter, we remark that this is similar to what happens in the theory and experiments of a drop of coherent atoms in a Bose-Einstein condensate trapped and subject to a double-welled tunneling potential [55, 56]

At this point one could ask if the low temperature experiments hold some information on the cell size for the proposed polycluster structure of glass, given that we have extracted values of the ATS concentration in the form of the quantity $n_{ATS} P^*$ (where n_{ATS} is the ATS number (mass) density) (see Tables). It is reasonable to assume, in fact, that on average four ATSS sit in each interstice between four tetrahedrally close-packed cells and this allows for a determination of the cell size ξ . If ξ is the cell's radius, the volume of the interstitial

space is $2\sqrt{2}\xi^3/3$ and therefore we have, on average:

$$\frac{4}{\frac{2\sqrt{2}}{3}\xi^3} = x_{ATS} = n_{ATS}\rho = \frac{n_{ATS}P^*\rho}{P^*} \quad (38)$$

where ρ is the solid's mass density. The parameter P^* could be determined, in principle, from the normalization condition for the ATS parameter distribution:

$$2\pi P^* \ln\left(\frac{D_{max}}{D_{min}}\right) \ln\left(\frac{D_{0max}}{D_{0min}}\right) = 1. \quad (39)$$

However D_{max} remains unknown from the fits to the data, so we can only make the reasonable guess that the quantity $\ln\left(\frac{D_{max}}{D_{min}}\right) \ln\left(\frac{D_{0max}}{D_{0min}}\right)$ is of order 1, to estimate $P^* \approx 1/(2\pi)$. We then get the estimating formula for the average cell radius

$$\xi \approx \left[\frac{3}{\pi\sqrt{2}(n_{ATS}P^*)\rho} \right]^{1/3} \quad (40)$$

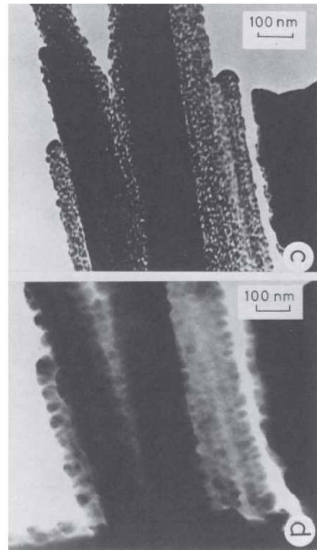
so that at this point we can use the values of $n_{ATS}P^*$ obtained in Section 3 to give cell size estimates. We use, for the silicates: $n_{ATS}P^* \approx 5 \times 10^{16} \text{ g}^{-1}$ (BAS glass), $9 \times 10^{16} \text{ g}^{-1}$ (Duran) and [as obtained in [42]] $1 \times 10^{16} \text{ g}^{-1}$ (BK7 glass). Then, from the literature [43] we get: $\rho \simeq 3.1 \text{ g cm}^{-3}$ (BAS glass), 2.3 g cm^{-3} (Duran) and 2.5 g cm^{-3} (BK7 glass). Using the above estimating formula Eq. (40) we arrive at the size of the cells in terms of their radius: $\xi \approx 1.63 \times 10^{-6} \text{ cm}$ or 163 \AA (BAS glass), $1.54 \times 10^{-6} \text{ cm}$ or 154 \AA (Duran) and finally $3.00 \times 10^{-6} \text{ cm}$ or 300 \AA (BK7 glass). Thus, from the low temperature experiments we get to estimate that for these silicates the cell size should be some 300 to 600 \AA in diameter (2ξ). Is this a reasonable estimate?

While high-resolution electron microscopy (HREM) images for the mentioned silicate glasses are not available in the literature, some HREM images of (inevitably) very thin samples of related glasses can be found. These are presented below, for the case of amorphous SiO_2 (Fig. 18(a)), amorphous $(\text{B}_2\text{O}_3)_{0.75}(\text{PbO})_{0.25}$ (Fig. 18(b)) and amorphous $\text{LiO}_2\cdot\text{SiO}_2$ (equimolar mixture, Fig. 18(c)). The cellular structure of these thin glass samples is clearly visible in these images, with the estimates for the diameter size $2\xi \approx 500 \text{ \AA}$, 600 \AA and, respectively, 500 \AA . While the second glass is not a silicate, the size of the cells as seen in HREM imaging for the two other silicates compares very favourably with the estimates for other silicates obtained from the low temperature work. It is therefore tempting to conclude that the estimate from the tunneling data at low temperatures lead to cellular sizes that are compatible with HREM imaging. This is also consistent with estimates for the number N of coherently tunneling atomic particles that make up each ATS. While N depends on temperature as stated, estimates [46] range from 10 to 10^2 and while the nature of the microscopic tunneling entities is still unknown and should depend on composition (in the case of pure SiO_2 this N should be close to 1) these values are not incompatible with a cell size of some 500 \AA in diameter. The question of the nature of the atomic coherently tunneling particles making up each ATS in each cellular interstice remains completely unanswered.

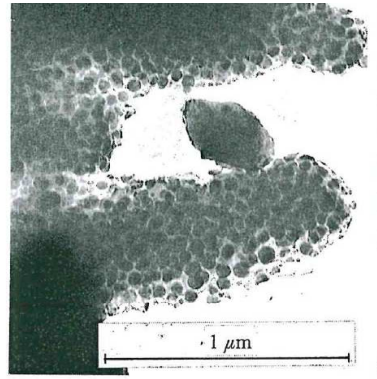
4.3 Conclusions

In conclusion, the cellular glass-structure backed ATS ETM for the magnetic effects in multi-component glasses (the multi-silicates BAS (or AlBaSiO), Duran and BK7) and contaminated mono-component vitreous glycerol has been fully justified in terms of a (not entirely) new vision for the intermediate-range structure of real glasses. In this scheme the particles are organized in regions of enhanced regularity (RERs) and more mobile *charged* particles trapped in the interstices (or cages) between the close-packed RERs. These are coherent (owing to proximity and strong Coulomb forces) atomic tunnelers that can be modeled in terms of single quasi-particles with highly renormalized tunneling parameters. This model explains a large number of experimental data and facts with remarkable consistency also in terms of cross-checks like the determination of the concentration of trace paramagnetic impurities [42].

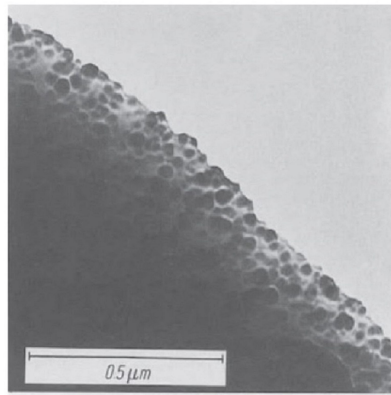
The fact that pure amorphous silica (Spectrosil-I, for example [45]) shows no detectable magnetic effects is a consequence of the extremely small size of the RERs for a- SiO_2 , deprived of almost any nucleation centres for both mosaic cells (RERs) and polycluster formation. These RERs will therefore trap a very small number N of dangling-bond ionic particles, or none at all given the covalent nature of the Si-O bonds. Hence, no magnetic effects are observable in this purest, single-component SiO_2 glass.



(a)



(b)



(c)

Figure 18: HREM images of the cellular structure of thin glass samples. (a) Amorphous SiO_2 (especially panel d, from [59], see also [60]), (b) amorphous $\text{B}_2\text{O}_3\text{-PbO}$ (from [60]), (c) amorphous $\text{Li}_2\text{O-SiO}_2$ (from [61]).

We remark at this point that the ETM with two types of TSs is not the only theoretical explanation that has been put forth for the explanation of the magnetic effects at low temperatures in the multi-silicate glasses.

It is however the only theory that successfully explains all of the experimental data so far, including those for the compositional effects, and that links the deviations from the STM to the real structure of glasses at the intermediate atomic range. Two other approaches have been in fact proposed to date, the one already mentioned based on the coupling of the 2LSs to nuclei in the sample carrying NEQMs [50] and the one based on the coupling of the 2LSs to paramagnetic Fe^{3+} impurities [62, 63]. These two other approaches have shortcomings that will not be discussed here, since their model justification has no bearing on the real atomic structure of glasses and on the glass-forming process from glass-forming liquids (the Zachariasen-Warren picture being – in fact – always tacitly assumed). Polymeric glasses should also be well described by the present cellular model (possibly also their surfaces [64]).

The present theory on the one hand bears heavily on the true structure of real glasses and it implies that the amorphous state should no longer be regarded as a dynamically arrested liquid, but rather as a new type of solid. It also shows on the other hand that the magnetic (and compositional) effects are a mere manifestation of the heterogeneous, cellular-type intermediate atomic structure of real glasses which abandons the Zachariasen-Warren picture for good. A cellular-type structure that has been advocated for by scientists, especially (but not only) in the ex-USSR, now for almost a century. It is not impossible that with this vision in mind the TSs could become in the near future the right probes with which to study the structure of real glasses in the laboratory.

Acknowledgements

The Author is very grateful to Maksym Paliienko and Silvia Bonfanti for their help with data fitting. He gratefully acknowledges stimulating discussions with A.S. Bakai. Part of this work was carried out whilst visiting the Physics Department of McGill University in Montreal (CA). The Author is grateful to Hong Guo for support and to him, to Martin Grant and Mark Sutton for useful discussions. On-going support from INFN-Pavia through Iniziativa Specifica GEOSYM-QFT is gratefully acknowledged.

References

[*] email: giancarlo.jug@uninsubria.it (corresponding author)

- [1] G. Jug: Theory of the Thermal Magnetocapacitance of Multi-component Silicate Glasses at Low Temperature, *Phil. Mag.* **84**(33), 3599–3615 (2004).
- [2] W.A. Phillips (Ed.): *Amorphous Solids: Low Temperature Properties*, (Springer Verlag, Berlin 1981).
- [3] P. Esquinazi (Ed.): *Tunneling Systems in Amorphous and Crystalline Solids* (Springer, Berlin, 1998).
- [4] W.H. Zachariasen: The Atomic Arrangement in Glass, *J. Am. Chem. Soc.* **54**, 3841–3851 (1932); *ibid.*: The Vitreous State, *J. Chem. Phys.* **3**, 162–163 (1935).
- [5] B.E. Warren: The Diffraction of X-Rays in Glass, *Phys. Rev.* **45**, 657–661 (1934).
- [6] W.M. MacDonald, A.C. Anderson and J. Schröder: Low-temperature Behavior of Potassium and Sodium Silicate Glasses, *Phys. Rev. B* **31**, 1090–1101 (1985).
- [7] G. Jug and M. Paliienko: Evidence for a Two-component Tunnelling Mechanism in the Multicomponent Glasses at low Temperatures, *Europhys. Lett.* **90** 36002 (2010).
- [8] C. Enss: Anomalous Behavior of Insulating Glasses at Ultra-Low Temperatures, *Adv. in Solid State Phys.* **42**, 335–346 (2002).
- [9] P. Strehlow, M. Wohlfahrt, A.G.M. Jansen, R. Haueisen, G. Weiss, C. Enss and S. Hunklinger: Magnetic Field Dependent Tunneling in Glasses, *Phys. Rev. Lett.* **84**, 1938–1941 (2000).
- [10] M. Wohlfahrt, P. Strehlow, C. Enss, and S. Hunklinger: Magnetic-Field Effects in Non-Magnetic Glasses, *Europhys. Lett.* **56**, 690–694 (2001); M. Wohlfahrt: Ph.D. Thesis (Heidelberg 2001, www.ub.uni-heidelberg.de/archiv/1587).
- [11] P. Nagel, A. Fleischmann, S. Hunklinger and C. Enns: Novel Isotope Effects Observed in Polarization Echo Experiments, *Phys. Rev. Lett.* **92**, 245511 (2004).
- [12] A.A. Lebedev: O Polimorfizme i Ozhighe Stekla, *Trud'i Gos. Opt. Inst.* **2** 1-20 (1921) (in Russian); *ibid.*, *Izv. Akad. Nauk SSSR, Otd. Mat. Estestv. Nauk, Ser. Fiz.* **3**, 381 (1937).
- [13] J.T. Randall, H.P. Rooksby and B.S. Cooper: The Diffraction of X-Rays by Vitreous Solids and its Bearing on their Constitution, *Nature* **125**, 438 (1930); *ibid.*: X-Ray Diffraction and the Structure of Vitreous Solids – I, *Z. Kristallogr.* **75**, 196–214 (1930).
- [14] E.A. Porai-Koshits: Genesis of Concepts on Structure of Inorganic Glasses, *J. Non-cryst. Sol.* **123**, 1–13 (1990).
- [15] A.C. Wright: Crystalline-like Ordering in Melt-quenched Network Glasses? *J. Non-cryst. Solids*, **401** 4–26 (2014); *ibid.*: The Great Crystallite versus Random Network Controversy: A Personal Perspective, *Int. J. Appl. Glass Sci.* **5**, 31–56 (2014).
- [16] A.S. Bakai: The Polycluster Concept of Amorphous Solids, Beck/Günterodt (Eds.), *Topics in Applied Physics* **72**, 209–255 (Springer-Verlag, Berlin Heidelberg 1994).
- [17] A.S. Bakai: *Poliklastern'ie Amorfn'ie Tela*, Khar'kov “Synteks” (Khar'kov, Ukraine 2013) (in Russian).
- [18] G. Adam and J.H. Gibbs: On the Temperature Dependence of Cooperative Relaxation Properties in Glass-Forming Liquids, *J. Chem. Phys.* **43**, 139–146 (1965).
- [19] L. Berthier and G. Biroli: Theoretical perspective on the glass transition and amorphous materials, *Rev. Mod. Phys.* **83**, 587–645 (2011).
- [20] C.A. Angell: Perspective on the Glass Transition, *J. Phys. Cem. Solids* **49**, 863–871 (1988).
- [21] V. Lubchenko and P.G. Wolynes: Theory of Structural Glasses and Supercooled Liquids, *Annu. Rev. Phys. Chem.* **58**, 235–266 (2007).

- [22] S.L. Simon and G.B. McKenna: Experimental Evidence Against the Existence of an Ideal Glass Transition, *J. Non-Cryst. Solids* **355**, 672–675 (2009).
- [23] G. Hägg: The Vitreous State, *J. Chem. Phys.* **3**, 284–49 (2016).
- [24] U. Satoshi and H. Koibuchi: Finsler Geometry Modeling of Phase Separation in Multi-Component Membranes, *Polymers* **8**, 284 (2016).
- [25] J. Hwang, Z.H. Melgarejo, Y.E. Kalay, I. Kalay, M.J. Kramer, D.S. Stone, P.M. Voyles: Nanoscale Structure and Structural Relaxation in $Zr_50Cu_45Al_5$ Bulk Metallic Glass, *Phys. Rev. Lett.* **108**, 195505 (2012).
- [26] M.M.J. Treacy and K.B. Borisenko: The Local Structure of Amorphous Silicon, *Science* **335**, 950–953 (2012).
- [27] J.C. Phillips: Realization of a Zachariasen Glass, *Solid State Comm.* **47**, 203–206 (1983).
- [28] M.M. Hurley and P. Harrowell: Kinetic Structure of a Two-dimensional Liquid, *Phys. Rev. E* **52**, 1694–1698 (1995).
- [29] H. Sillescu: Heterogeneity at the Glass Transition: a Review, *J. Non-Cryst. Solids* **243**, 81-108 (1999).
- [30] M.D. Ediger: Spatially Heterogeneous Dynamics in Supercooled Liquids, *Annu. Rev. Phys. Chem.* **51**, 99–128 (2000).
- [31] K. Vollmayr-Lee and A. Zippelius: Heterogeneities in the Glassy State, *Phys. Rev. B* **72**, 041507 (2005); K. Vollmayr-Lee, W. Kob, K. Binder and A. Zippelius: Dynamical heterogeneities below the glass transition, *J. Chem. Phys.* **116**, 5158–5166 (2002).
- [32] C. Donati, S.C. Glotzer, P.H. Poole, W. Kob and S. Plimpton: Spatial Correlations of Mobility and Immobility in a Glass-forming Lennard-Jones Liquid, *Phys. Rev. E* **60**, 3107–3119 (1999).
- [33] P.-G. de Gennes: A Simple Picture for Structural Glasses, *Comptes Rendus - Physique* **3**, 1263–1268 (2002).
- [34] H.P. Baltes: A Cellular Model for the Specific Heat of Amorphous Solids at Low Temperatures, *Solid State Commun.* **13**, 225–228 (1973).
- [35] W.A. Phillips: Two-level States in Glasses, *Rep. Prog. Phys.* **50**, 1657–1708 (1987).
- [36] J. A. Sussmann: Electric Dipoles due to Trapped Electrons, *Proc. Phys. Soc. (London)* **79**, 758–774 (1962).
- [37] G. Jug and M. Paliienko: Multilevel Tunneling Systems and Fractal Clusters in the Low-Temperature Mixed Alkali-Silicate Glasses, *Sci. World J.* **2013**, 1–20 (2013).
- [38] G. Jug: Multiple-well Tunneling Model for the Magnetic-field Effect in Ultracold Glasses *Phys. Rev. B* **79**, 180201 (2009).
- [39] G. Jug, M. Paliienko and S. Bonfanti: The Glassy State Magnetically Viewed from the Frozen End, *J. Non-Cryst. Solids* **401**, 66–72 (2014).
- [40] C. C. Yu and A. J. Leggett: Low Temperature Properties of Amorphous Materials: Through a Glass Darkly, *Comm. Cond. Mat. Phys.*, **14**, 231–? (1988).
- [41] G. Jug, S. Bonfanti and W. Kob: Realistic Tunneling Systems for the Magnetic Effects in non-metallic Real Glasses, *Phil. Mag.* **96**, 648–703 (2016).
- [42] S. Bonfanti and G. Jug: On the Paramagnetic Impurity Concentration of Silicate Glasses from Low-Temperature Physics *J. Low Temp. Phys.* **180**, 214-237 (2015).
- [43] L. Siebert: Ph.D. Thesis Heidelberg University (2001), www.ub.uni-heidelberg.de/archiv/1601

- [44] H.M. Carruzzo, E.R. Grannan and C.C. Yu: Non-Equilibrium Dielectric Behavior in Glasses at Low Temperatures: Evidence for Interacting Defects, *Phys. Rev. B* **50**, 6685–6695 (1994).
- [45] S. Ludwig, P. Nagel, S. Hunklinger and C. Enss: Magnetic Field Dependent Coherent Polarization Echoes in Glasses, *J. Low Temp. Phys.* **131**, 89–111 (2003).
- [46] M. Paliienko: Multiple-welled Tunnelling Systems in Glasses at low Temperatures (Ph.D. Thesis, Università degli Studi dell’Insubria, 2011) <http://insubriaspacespace.cineca.it/handle/10277/420>
- [47] F. LeCochech, F. Ladieu and P. Pari: Magnetic field effect on the dielectric constant of glasses: Evidence of disorder within tunneling barriers, *Phys. Rev. B* **66**, 064203 (2002).
- [48] B.P. Smolyakov and E.P. Khaimovich, (courtesy A. Borisenko) *Pis'ma Zh. Eksp. Teor. Fiz.* **29**, 464 (1979) (in Russian); *ibid.*: Dynamic processes in dielectric glasses at low temperatures, *Sov. Phys. Uspekhi*, **25**, 102115 (1982).
- [49] S. Ludwig, P. Nagel, S. Hunklinger and C. Enss: Direct Coupling of Magnetic Fields to Tunneling Systems in Glasses, *Phys. Rev. Lett.* **88**, 075501 (2002).
- [50] A. Würger, A. Fleischmann and C. Enss: Dephasing of Atomic Tunneling by Nuclear Quadrupoles, *Phys. Rev. Lett.* **89**, 237601 (2002).
- [51] J.L. Black and B.I. Halperin: Spectral Diffusion, Phonon Echoes and Saturation Recovery in Glasses at Low Temperatures, *Phys. Rev. B* **16**, 2879–2895 (1977).
- [52] V.L. Gurevich, M.I. Muradov and D.A. Parshin: Electric Dipole Echo in Glasses, *Sov. Phys. JETP* **70**, 928 (1990).
- [53] Yu.M. Galperin, V.L. Gurevich and D.A. Parshin: Nonlinear Resonant Attenuation in Glasses and Spectral Diffusion, *Phys. Rev. B* **37**, 10339–10349 (1988).
- [54] C. Enss, S. Ludwig, R. Weis and S. Hunklinger: Decay of Spontaneous Echoes in Glasses, *Czechoslovak J. Phys.* **46**, 2247–2248 (1996).
- [55] A. Smerzi, S. Fantoni, S. Giovanazzi, and S. R. Shenoy: Quantum Coherent Atomic Tunneling between Two Trapped Bose-Einstein Condensates, *Phys. Rev. Lett.* **79**, 4950 (1997).
- [56] M. Albiez, R. Gati, J. Fölling, S. Hunsmann, M. Cristiani and M.K. Oberthaler: Direct Observation of Tunneling and Nonlinear Self-Trapping in a Single Bosonic Josephson Junction, *Phys. Rev. Lett.* **95**, 010402 (2005).
- [57] D. Simatos, G. Blond, R. Roudaut, D. Champion, J. Perez and A.L. Faivre: Influence of Heating and Cooling Rates on the Glass Transition Temperature and the Fragility Parameter of Sorbitol and Fructose as measured by DSC, *J. Thermal Analysis* **47**, 1419–1436 (1996).
- [58] J. Buchholz, W. Paul, F. Varnik and K. Binder: Cooling Rate Dependence of the Glass Transition Temperature of Polymer Melts: Molecular Dynamics Study, *J. Chem. Phys.* **117**, 7364–7372 (2002).
- [59] J. Zarzycki: *Proc. X Intern. Congress on Glass*, Kyoto, Japan, No. 12, p. 28 (1974).
- [60] J. Zarzycki: *Glasses and the Vitreous State* (Cambridge University Press, Cambridge 1991), p. 172.
- [61] W. Vogel: *Glasses Chemistry* (Springer-Verlag, Berlin 1992) 2nd edition, p. 74.
- [62] A. Borisenko: Hole-compensated Fe³⁺ Impurities in Quartz Glasses: a Contribution to Subkelvin Thermodynamics, *J. Phys.: Condens. Matter*, **19**, 416102 (2007) .
- [63] A. Borisenko and G. Jug: Paramagnetic Tunneling Systems and Their Contribution to the Polarization Echo in Glasses, *Phys. Rev. Lett.* **107**, 075501 (2011).
- [64] E. Proutorov and H. Koibuchi: Orientation Asymmetric Surface Model for Membranes: Finsler Geometry Modeling, *Axioms* **6**, 10 (2017).